UNIFIED SECONDARY AND TERTIARY CREEP MODELING OF ADDITIVELY MANUFACTURED NICKEL-BASED SUPERALLOYS

by

Harshal Ghanshyam Dhamade

A Thesis

Submitted to the Faculty of Purdue University

In Partial Fulfillment of the Requirements for the degree of

Master of Science in Mechanical Engineering

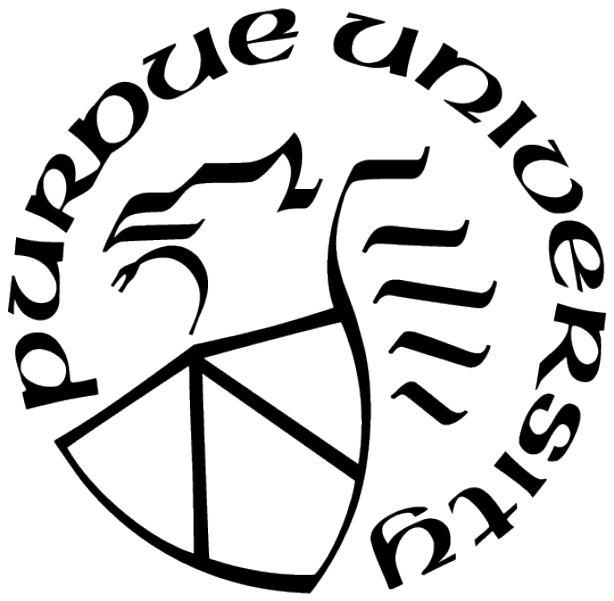

Department of Mechanical and Energy Engineering

Indianapolis, Indiana

August 2021

THE PURDUE UNIVERSITY GRADUATE SCHOOL
STATEMENT OF COMMITTEE APPROVAL

Dr. Jing Zhang, Chair

Department of Mechanical and Energy Engineering

Dr. Andres Tovar

Department of Mechanical and Energy Engineering

Dr. Khosrow Nematollahi

Department of Mechanical and Energy Engineering

Approved by:

Dr. Jie Chen

Dedicated to the loving memory of my Father, Ghanshyam Shankar Dhamade.

ACKNOWLEDGMENTS

I would like to express sincere gratitude to my advisor Dr. Jing Zhang for his patience, motivation, and providing constant guidance and being an incredible source of knowledge throughout my research work. He provided me with unequivocal support to achieve my goals and was patient through my errors. His constant encouragement helped me get the National Science Foundation grants and helped me present papers in several conferences of repute. I would also like to thank Dr. Andres Tovar, and Dr. Khosrow Nematollahi for their support during my time at the university, sharing their thoughts and feedback which helped me broaden my perspective of research work and for serving as part of my advisory committee.

I would like to thank IUPUI and entire staff of the Department of Mechanical and Energy Engineering for providing support and assistance during various stages of my research. Special thanks to Linda Wright and Jerry Mooney for their support and motivation throughout my time at IUPUI. I would like to thank my lab mates, Swapnil, Tejesh, Abhilash, Anudeep, Sagar, Jian, Xuehui and Lingbin among others for all their help and banter. Last, but not the least, I would like to thank my mother Sunita Ghanshyam Dhamade for believing in me, my sister Pooja for her emotional support and my uncle and aunt Nilkanth and Sandhya Dhamade for supporting me both financially and emotionally, along with my siblings Akash, Kajal, Ashish and friends Vighnesh, Durvesh, Dewant, Akash, Shantanu, Amrut, Bhakti, Shailesh, Wardhan, Karishma and Sowmya for always standing by my side.

TABLE OF CONTENTS

LIST OF TABLES

LIST OF FIGURES

LIST OF SYMBOLS

σ	Stress
σ_{eq}	Equivalent Stress
σ_{net}	Net/Effective Stress
σ_{rup}	Rupture Stress
ε	Strain
ε_{cr}	Creep Strain
$\dot{\varepsilon}_{cr}$	Creep Strain Rate
ω	Damage
t	Time
T	Temperature
A	Secondary creep material constant
m	Temperature dependent primary creep exponent
n	Temperature dependent secondary creep exponent
B	Tertiary creep material constant for Kachanov-Rabotnov
M	Tertiary creep material constant for Liu-Murakami
χ	Tertiary creep material constant
ϕ	Tertiary creep damage constant for Kachanov-Rabotnov
q_2	Tertiary creep damage constant for Liu-Murakami

ABBREVIATIONS

CDM	Continuum Damage Mechanics
K-R	Kachanov-Rabotnov
L-M	Liu-Murakami
AM	Additively Manufactured
TM	Traditionally Manufactured
SS	Stainless Steel
SET	Single Element Test
FEM	Finite Element Method
SLM	Selective Laser Melting
L-PBF	Laser Powder Bed Fusion
IGT	Industrial Gas Turbine
HIP	Hot Isostatic Pressing

ABSTRACT

Additively manufactured (AM) metals have been increasingly fabricated for structural applications. However, a major hurdle preventing their extensive application is lack of understanding of their mechanical properties. To address this issue, the objective of this research is to develop a computational model to simulate the creep behavior of nickel alloy 718 manufactured using the laser powder bed fusion (L-PBF) additive manufacturing process. A finite element (FE) model with a subroutine is created for simulating the creep mechanism for 3D printed nickel alloy 718 components.

A continuum damage mechanics (CDM) approach is employed by implementing a user-defined subroutine formulated to accurately capture the creep mechanisms. Using a calibration code, the material constants are determined. The secondary creep and damage constants are derived using the parameter fitting on the experimental data found in literature. The developed FE model is capable to predict the creep deformation, damage evolution, and creep-rupture life. Creep damage and rupture is simulated as defined by the CDM theory. The predicted results from the CDM model compare well with experimental data, which are collected from literature for L-PBF manufactured nickel alloy 718 of creep deformation and creep rupture, at different levels of temperature and stress.

Using the multi-regime Liu-Murakami (L-M) and Kachanov-Rabotnov (K-R) isotropic creep damage formulation, creep deformation and rupture tests of both the secondary and tertiary creep behaviors are modeled.

A single element FE model is used to validate the model constants. The model shows good agreement with the traditionally wrought manufactured 316 stainless steel and nickel alloy 718 experimental data collected from the literature. Moreover, a full-scale axisymmetric FE model is used to simulate the creep test and the capacity of the model to predict necking, creep damage, and creep-rupture life for L-PBF manufactured nickel alloy 718. The model predictions are then compared to the experimental creep data, with satisfactory agreement.

In summary, the model developed in this work can reliably predict the creep behavior for 3D printed metals under uniaxial tensile and high temperature conditions.

1. INTRODUCTION

Manufacturing metal components using Additive Manufacturing (AM) has popularized in many industrial sectors in recent years. Yet predicting the behavior of 3D printed metals under extensive loading conditions and high-temperature environments, such as in Gas Turbines and pressure vessels, is still poorly understood as compared to the traditionally manufactured counterparts. Creep properties are critical for metals used in a high-temperature environment such as Industrial Gas Turbine Blades. Thus, requiring the need to better understand the creep behavior of 3D printed metals.

1.1 Motivation

Creep properties are critical for metals used in a high-temperature environment. For example, industrial gas turbines and aircraft gas turbine engines which usually consist of rotating turbine blades that are operated at very high temperatures. Modern turbine blades are often made of nickel-based super alloy materials that incorporate chromium, cobalt, and rhenium. The blades extract energy from the high temperature, high-pressure gas produced by the combustor. Blade fatigue and creep are a major source of failure in gas turbines. Due to the stress induced by vibration and resonance within the operating range of machinery fatigue is induced and over time due to high temperatures and stresses creep failure is caused. To determine the state of the turbine components and to schedule the inspection, maintenance, and replacement periods, creep prediction models are used. To avoid over maintenance, lay off time, and premature replacement of components, and to reduce the overall cost, accurate creep prediction models are required.[5] There are various models available to predict multiple creep stages and every model is developed on a different assumption. Although, it is very important to have a set of constitutive equations to predict the creep phenomena and be accurate and easy for application.[5]

Generally, the turbine blades are exposed to external as well as internal damages. The external surfaces are damaged due to factors like corrosion, oxidation, crack formation, erosion, etc. and the internal damage of micro structure include phase change, grain growth, brittle phase formation, creep, and grain boundary void formation.[18] According to a study

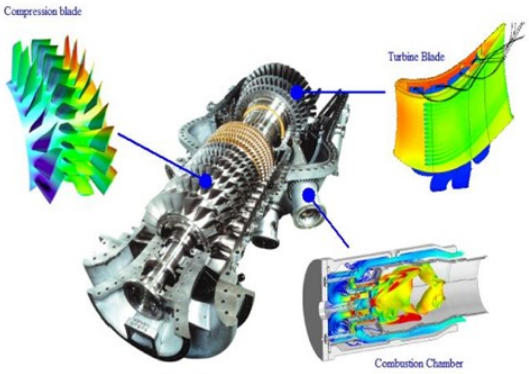

Figure 1.1. IGT and the components subjected to failure.[5]

conducted on gas turbines failure by Blotch (1982), it was concluded that turbine blades and rotor components contribute almost 25 percent as a primary cause of gas turbine failure. Another study showed that creep, high cycle fatigue (HCF), and turbine blade cooling related failures contributed more than 50 percent towards the total damage costs for IGTs.[18] Components for such applications are comprised of primary creep resistant materials such as Ni-base super alloys. Although, primary creep is generally negligible while the secondary and tertiary creep regimes dominate the creep life. These types of creep lives are highly nonlinear. It is important to accurately predict life.

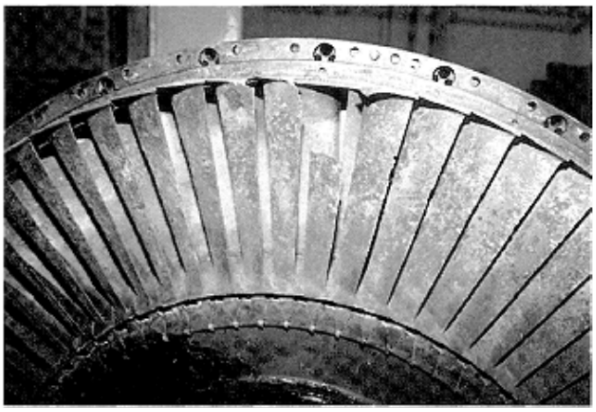

Figure 1.2. Creep, corrosion, and fatigue failure at the tip due to rubbing.[5]

Nickel-base super alloys are excellent candidate materials for turbine blades, transition pieces, vanes, turbine discs, combustors, and boilers due to high-temperature strength, corrosion resistance, and oxidation resistance.[25] Creep is the inelastic deformation of a material

at a high temperature. Typically, this form of strain of Ni-base super alloys is predicted via either steady-state (e.g., secondary) creep deformation modeling with or without consideration of the tertiary creep regime. As temperature increases, the creep strain rate increases accordingly.[24] For applications where Ni-based super alloys are used at high temperatures, predicting the creep behavior reduces the maintenance downtime as well as the cost of maintenance. With the increase in usage of 3D printing in high temperature and energy applications, it is critical to have a characterized numerical model that would incorporate the damage and rupture evolution and prediction. Understanding the creep behavior of 3D printed parts and to characterize the parameters associated with creep damage leading to rupture or crack propagation would further reinforce the use of additive manufacturing processes.[32]

1.2 Objective

The objective of this thesis is to develop a continuum damage mechanics (CDM) model to understand the creep failure in Ni-based superalloys and advance the knowledge of creep behavior of nickel alloy 718 manufactured through laser powder bed fusion (L-PBF). A finite element model based on continuum damage mechanics including a damage evolution model is developed to predict the creep life. Extensive literature review on short term and long term creep life of metals lead to the proposal of the following research tasks:

1. Selection of CDM model: Based on the background literature study of the existing popular creep model, advantages and limitations are discussed. Characteristics of the model, material calibration with experimental data fitting are discussed in detail.

2. Numerical Analysis: Uniaxial creep rupture test data collected from literature are used to determine the material parameters for the selected CDM model. Traditionally manufactured (TM) nickel alloy test data is used to validate the curve fitting process and constants are calculated for the SLM manufactured nickel alloy 718.

3. User Subroutine Development: The CDM model is formulated using a FORTRAN user subroutine for ABAQUS solver. Single element testing is performed for applied stress and displacement to validate the subroutine.

4. FEM simulation: A series of finite element simulations on a cylindrical specimen are conducted. ABAQUS is used to perform the quasi-static FE simulations.

1.3 Structure of Thesis

The present work is divided into seven sections. The first chapter consists of an introduction to the thesis which includes the motivation, objective, and overall structure of the thesis.

The second chapter reviews literature that is relevant to the creep deformation mechanism in metals and creep damage. Popular models available in generalized FEM solvers are studied. It contains an overview of existing work on constitutive models for different creep stages and isotropic creep damage models. The concept of creep deformation, time-dependent plasticity, and damage mechanics is explored.

The third chapter deals with the material used in this thesis. Creep properties and experimental test data for traditionally manufactured (TM) and additive manufactured (AM) Ni-based superalloys are compared.

The fourth chapter consists of the material calibration procedure to calculate the creep and damage variables used in the CDM. Popular single parameter damage mechanics model Kachanov-Rabotnov model, its limitation, and Liu-Murakami, another damage model, and its advantages are discussed. Material constants are estimated for the material used in the work.

The fifth chapter models the creep behavior utilizing the user subroutine. A user subroutine code is developed based on the CDM models discussed in the previous chapter. Single element testing is performed to study the effect of various constants on the creep life prediction capability of the subroutine. Damage evolution with and without rupture is explored along with its limitations.

The sixth chapter covers the finite element study of the CDM models. FEM simulations for a flat and cylindrical specimen using ABAQUS are conducted for KR and LM models. Detailed comparison and discussion of these two models are provided for TM and AM Ni-based superalloy samples.

Finally, chapter seven concludes the findings of this study and the eighth chapter would recommend future work associated with this research.

2. BACKGROUND

2.1 Additive Manufacturing

Turbomachinery is crucial for the energy generation industry. Its high-performance parts feature complex designs that need to be robust and powerful as the demand for energy increases. Besides, turbomachinery parts need to be resistant and reliable – even at temperatures beyond the melting point. Additive manufactured turbine parts enable higher combustion temperatures and reduce maintenance times. During operation, the turbomachinery parts are subjected to failure mechanisms like fatigue, creep, corrosion, erosion, etc. and have a severe impact on the safety and reliability of the machine. 3D printing metal parts for turbomachinery like blades, vanes, inlet/outlet, etc. not only aids in manufacturing complex parts but can be incorporated with an optimized cooling strategy to achieve desired material properties and make material failure resistant.

Numerical modeling to predict material failure under deformations such as creep, fatigue, crack propagation for 3D printed specimen has picked up in the last few years. An immense number of models have been developed to predict the deformation, damage evolution, and rupture of structural alloys subjected to creep and creep-fatigue. Stewart [25] conducted experiments to develop a numerical model with temperature dependence of tertiary creep damage of a Ni-based alloy. Haque [5] compared the creep prediction capability of the Sine-Hyperbolic and the classical Kachanov-Rabotnov creep damage models. The models were fit to creep data for stainless steel 304. Hautfenne [7] studied the influence of heat treatments and build orientation on SLM manufactured nickel alloy 718 specimens. Short term creep tests were performed and the creep curves were compared with conventionally produced nickel alloy 718 creep behavior.

Another study by Kuo [13] showed the effect of post-processing on the microstructure dependent creep properties of nickel alloy 718 manufactured by SLM. Xu [29] studied the creep performance of laser powder bed fusion manufactured nickel alloy 718 specimens and compared with conventional hot-rolled, as-built then heat treated and as-built then HIPed specimens. An increased secondary creep rate was correlated with a reduced life. In a similar study by Kreitcberg [12] mechanical properties of nickel alloy 625 manufactured by

LPBF and post processed by annealing and HIPing were studied. Creep tests conducted at 760 °C under 0.5-0.9 yield stress condition showed a distinguishable three stage creep behavior for low to medium yield stress. Creep behavior of LPBF manufactured alloy 718 parts fabricated using different scanning strategies and build orientations was studied by Sanches.[20] Creep tests were performed at 650 °C under a 600 MPa load. It was found out that heat treatment increased the creep life by a factor of 5 and build orientation and stress state was a determining factor in the creep failure mechanism.

2.1.1 Laser powder bed fusion (L-PBF)

Laser powder bed fusion is a rapid prototyping (Additive manufacturing) process which selectively melts the powder bed which is a thin layer of powdered metal using a laser according to a 3D CAD model. Once the layer is solidified, a new layer is spread and the process repeats until the part is formed.[30]

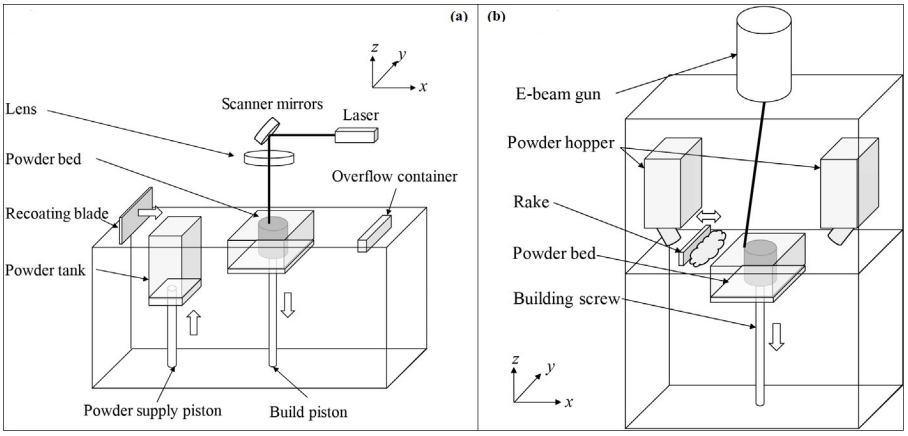

Figure 2.1. Schematic representation of powder bed fusion equipment (a) selective laser melting (b) electron beam melting.[32]

In the L-PBF process, the laser beam passes through a system of lenses and is reflected by a mirror onto the platform surface. The laser beam spot movement in the X-Y plane is controlled by the mirrors as per the CAD.[31] After one layer of powder solidifies, the platform moves down, and a re-coating blade or brush pushes a fresh layer of powder from the powder dispenser. The laser scanning processes is repeated as per the provided CAD

input and the re-coating and laser scanning continues. The build chambers for these machines are filled with an inert gas to avoid oxidation of the metal as it melts and solidifies.[32]

L-PBF produces dense metal components directly from CAD data without a need for tooling.[27] When compared to a fused deposition modeling (FDM) process, L-PBF has many advantages like ability to 3D print metals, lack of support structure requirement, wide range of materials that can be processed. However, there are certain challenges with L-PBF which include high material cost, slow speed, laborious post-processing requirements and material compatibility issues.[3]

2.2 Fundamentals of Creep

When metals are subjected to stress at an elevated temperature, usually above 0.4 times the absolute melting temperature, a time-dependent deformation occurs called Creep.[28] Creep represents the plastic flow of metals with time under constant load and temperature. Generally, in metals creep is a type of deformation that occurs at stresses below the yield strength of the material.[25] Yield strength defines the stress at which metal deforms plastically. When undergoing creep deformation, metals strain plastically even though yield stress is not reached.

Constant load tests are performed on a uniaxial test specimen to obtain creep data. The strain versus time response is usually referred to as a creep curve. For a specimen subjected to a state of constant uniaxial stress, a typical creep curve can be calculated. The creep curve can be divided into three distinct regions i.e., a region of increasing strain rate (the primary creep), a region of constant strain rate (the secondary creep), and a region of accelerating strain rate (the tertiary creep), which leads to rupture.[28]

Creep behavior is mainly dependent on the applied stress, temperature, and creep strain. Figure 2.3 (a) and (b) show the general trend of creep behavior with changing stress and temperature, respectively.

Rupture time and rupture strain, which is a measure of materials ductility, are affected by temperature as can be seen in Figure 2.4.

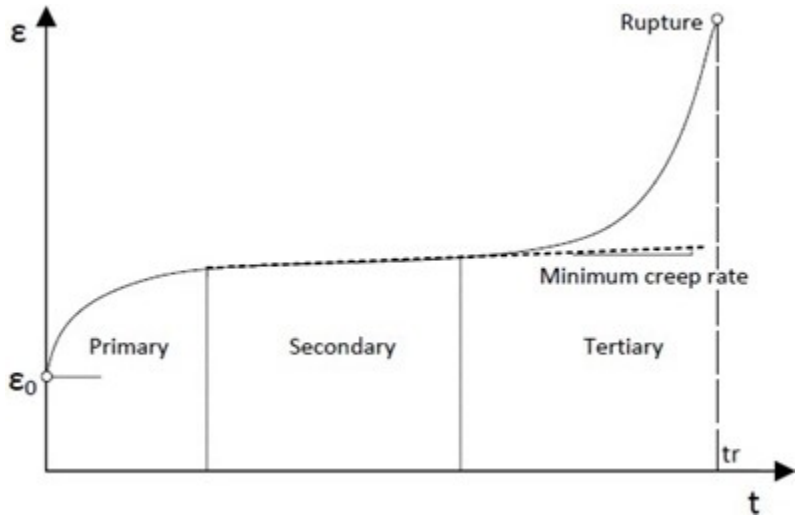

Figure 2.2. Creep strain versus time, a typical creep curve.[28]

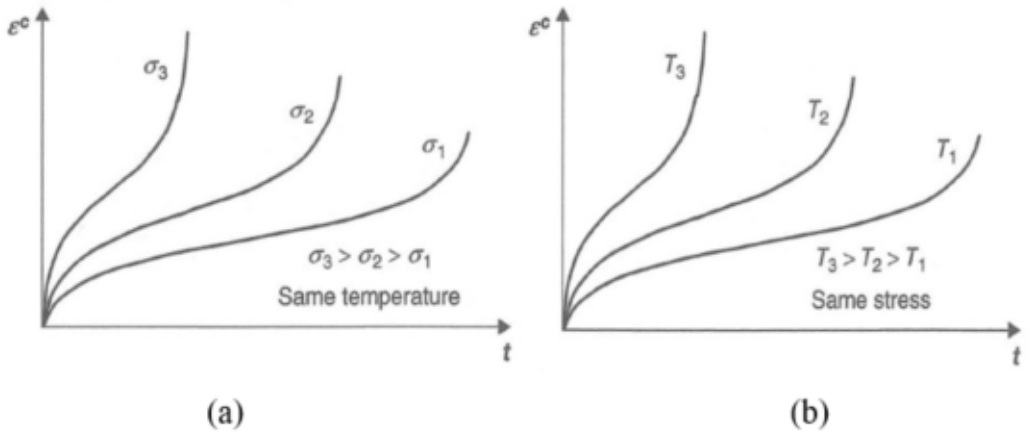

Figure 2.3. Effect of (a) Stress and (b) temperature on creep behavior.[28]

Stress response of metals under elevated temperatures are highly complex and non-linear. For some metals under certain loading conditions, the creep response can be even more complex. For example, stainless steel 316 at 550°C, as shown in Figure 2.5, exhibits a renewed primary and secondary creep behavior for stresses less than 300 MPa.[28]

Microstructural changes that occur as a result of aging due to the exposure to elevated temperature for the period of time and stress causes the renewed primary and secondary creep.

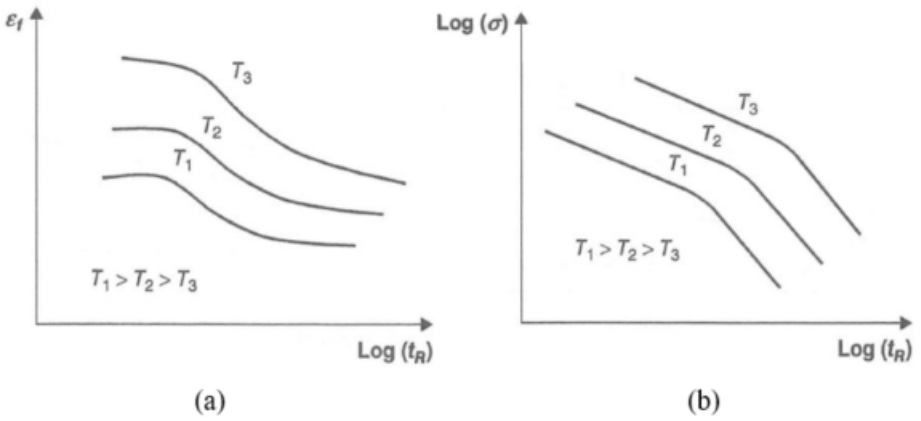

Figure 2.4. Effect of temperature on (a) log of rupture strain vs log of time to rupture and (b) log of stress vs log of time to rupture.[28]

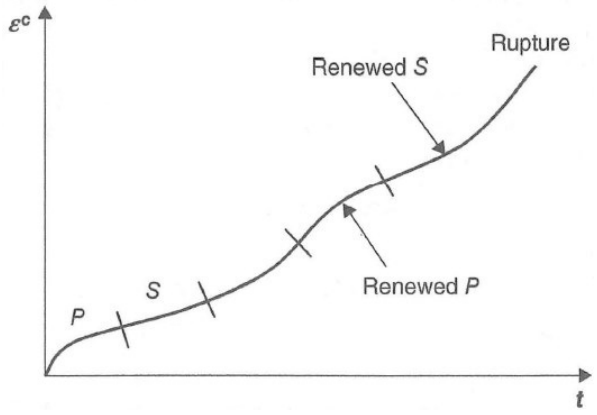

Figure 2.5. Anomalous creep behavior of stainless steel 316 at 550°C for stresses below 300MPa.[28]

2.3 Constitutive Model for Creep Stages

A creep constitutive model can be considered as a viscoplasticity model where the yield surface is zero.[24] They can be further divided into two types, mechanistic and phenomenological. Mechanistic constitutive models relate to fundamental microstructure mechanism (micro/nanoscale creep) and focus on determining creep strain-stress relationship. Phenomenological constitutive models on the other hand focus on determining bulk creep strain-stress relationship by relating to functional relations. Microstructural mechanisms are not considered in this type of constitutive model when looking at a macro scale creep.[25]

To possess good creep resistance, a material should have metallurgical stability under long-term high-temperature exposure, resistance to oxidation and corrosive media, and a large grain size that reduces the grain boundaries.[5] In superalloys, pre-existing dislocations encounter obstacles such as precipitates, solid solution atoms, grain boundaries, etc. and become immobile causing strain hardening and eventually subjected to primary creep.[24]

The primary creep stage is a short-lived phenomenon for Ni-based superalloys and can be neglected in constitutive modeling as the deformation at this stage is very small compared with the total deformation.[5] The secondary stage is characterized by a constant strain rate due to the balance between strain-hardening and recovery mechanics. Temperature-induced diffusion where dislocations can diffuse away from obstacles and the nucleation of grain boundaries and grain boundary sliding occurs during this transient stage.[22] And finally, tertiary creep takes over and is characterized by a nonlinear increase of strain rate until creep rupture. In ductile materials, a net area reduction due to elongation is seen and the evolution of this phenomenon is called damage. It affects the material creep strength.[24]

Total strain can be divided into plastic, elastic, and creep strain components as shown below:

$$\varepsilon_{total} = \varepsilon_{elastic} + \varepsilon_{plastic} + \varepsilon_{creep} \tag{2.1}$$

instantaneous plastic strain and inelastic strains are neglected. The identification of the dominant creep mechanism under various boundary conditions can be done using deformation mechanism maps.

To define the physical mechanism of creep in metals, crystal lattice defines the mean position and atoms within a solid vibrate. As temperature increases, the amplitude of vibration increases, and eventually causes the atom to diffuse within the lattice structure. The spacing between atoms is large and irregular at grain boundaries than within the grains, which leads to formation of weak regions with dislocations initiating and terminating at those sites. Vacancies also diffuse to and from grain boundaries which further leads to weakening of those boundaries. To overcome the dislocations within the grains and grain boundaries, introduction of obstacles during the manufacturing and heat treatment process help stop or

slow down the movement of the vacancies. The dislocations move past these obstacles by a dislocation climb process. It is observed that, in such cases, the precipitates can dissolve and cause a creep strengthening effect to reduce.

General creep behavior of materials and the relationship between creep strain rate components and equivalent creep strain rate.[21] However, creep behavior models can be classified into three broad categories,

- **Secondary Creep behavior model**: Creep models define secondary creep behavior like Norton Power law.
- **Tertiary Creep behavior model**: Damage mechanics models capable of predicting secondary and tertiary behavior and failure times like Kachanov-Rabotnov single-damage parameter model, Liu-Murakami single damage parameter model, and Dyson two damage parameter model.
- **Unified material behavior model**: Models used to represent rate-dependent plasticity, stress-relaxation, and cyclic stress-strain behavior like Chaboche viscoplastic model.

2.3.1 Primary Creep Modeling

Primary creep is transient in nature thus making it time dependent. There are numerous phenomenological primary creep equations that have been developed. Andrade's law for primary creep is one of the most popular one.[25]

$$\varepsilon_{cr} = \varepsilon_0 + At^{1/q} \tag{2.2}$$

Where ε_0 is the instantaneous creep , A and $t^{1/q}$ is a coefficient, and q is a unitless exponent. Another formulation for primary creep is the power law of the simple form:

$$\varepsilon_{cr} = A\sigma^n t^m \tag{2.3}$$

Where σ is load and A ($MPa^{-n}hr^{-m}$), n, and m are temperature dependent constants.

In the case of Ni-based alloys, the primary creep stage is short compared to rupture strain. For example, creep deformation curves for a wrought Ni-base alloy 617 are provided in Figure 2.6

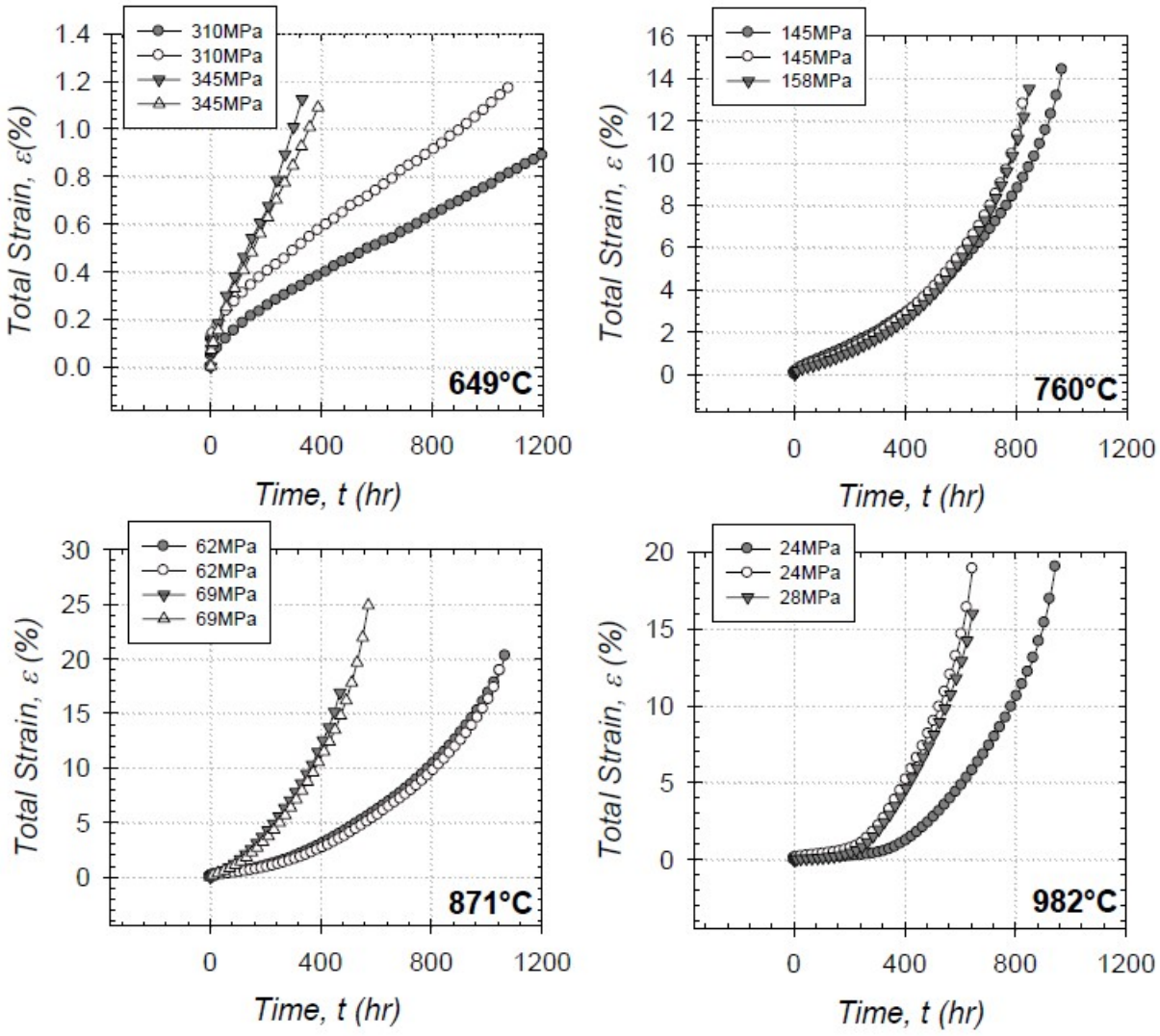

Figure 2.6. Creep deformation curves for nickel alloy 617.[3]

For IN617 at the temperature 649°C (approximately 0.5 T_m) primary creep is observable as strain hardening before the onset secondary creep. At 760, 871, and 982°C, the importance of modeling primary creep is reduced. As temperature increases, the contribution of primary creep to the final rupture strain becomes negligible.[24]

2.3.2 Secondary Creep Modeling

Secondary creep stage also known as steady state creep is a constant strain rate region in the creep curve. It represents a transition from primary to tertiary creep.[25] The classical approach to modeling the secondary creep behavior for materials is the Norton power law for secondary creep:

$$\dot{\varepsilon}_{cr} = \frac{d\varepsilon_{cr}}{dt} = A\sigma^n \tag{2.4}$$

Where A and n are secondary creep constants and σ is equivalent stress. Typically, von mises stress which is both isotropic and pressure insensitive are used. The Norton power law is sometimes referred to as the Norton-Bailey law. The secondary creep constants A and n exhibit temperature-dependence. Stress provides a substantial contribution to the creep strain rate as the n secondary creep constant is an exponent of stress.[24]

2.3.3 Tertiary Creep Modeling

Tertiary regime comprises of a sudden increase of strain rate. A rapid increase in creep deformation consistent with the microstructural degradation eventually leads to rupture. Creep damage at a microstructural level can occur in a number of ways, such as microcracks, cavities, voids, etc. Typically, creep damage is classified into two forms: trans-granular (ductile) damage and intergranular (brittle) damage. Trans-granular (ductile) damage arises were slip bands of plasticity forming under high stress and low temperature. Intergranular (brittle) damage is a microcracking process at grain boundaries under high temperature and low stress.[25]

Damage is non-recoverable phenomenon which is dependent on material behavior (i.e., creep constants), temperature, time, and stress. Generally, damage is considered to be in continuum, (i.e., homogenous thought a body) thereby the expression continuum damage mechanics (CDM) is used. Creep damage is modeled using continuum damage mechanics, where micro-scale damage is modeled as a homogenous macro-scale effective constitutive response within a finite volume.[24]

Continuum damage mechanics was first introduced by Kachanov, who introduced a continuity factor to describe the degree of material degradation and predicted the creep rupture life of polycrystalline metals. Then, Rabotnov extended the concept of continuity, introduced the damage variable, and defined the effective stress, which makes it possible for the coupling of strain and damage.[17]

- **Creep Damage**: Creep damage can be considered equal to the reduction-in-area from microcrack, cavities, voids, and etc. as a structure undergoes creep deformation. As shown in Figure 2.7, the physical space includes voids and dislocations which represents damage.

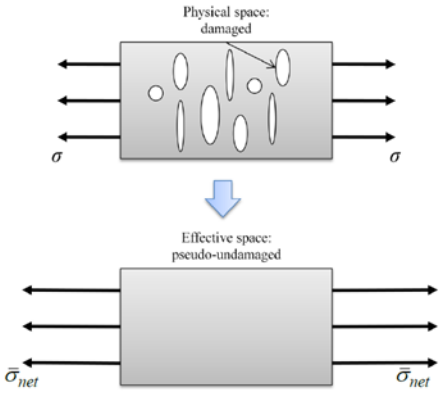

Figure 2.7. Schematic representation of the concept of physical and effective space.[25]

Now if we consider a volume without any voids, known as an effective space, the force applied to the undamaged area is a function of a damage parameter which compensates for the assumption of no void/defect (physical space). This reduction-in area can be represented mathematically as the net/effective stress.[25]

$$\bar{\sigma}_{net} = \tilde{\sigma}\frac{A_0}{A_{net}} = \frac{\tilde{\sigma}}{1 - \frac{A_0 - A_{net}}{A_0}} = \frac{\tilde{\sigma}}{(1-\omega)} \tag{2.5}$$

where A_{net} is the current area, A_0 is the initial area, $\tilde{\sigma}$ is equivalent stress, $\bar{\sigma}_{net}$ is the net/effective stress, and ω is damage. The effective stress increase leads to an accelerated rate of creep deformation. The physical damage is thus replaced with an effective increase in the applied stress.[24]

- **Creep Rupture**: Creep rupture, or stress rupture occurs in materials with a permanent high load which is acting on them and leads to failure due to creep. Creep continuum damage is usually observed in metallic specimen tested under constant stress and temperature condition for long time periods. Damage was observed to grow along the planes perpendicular to the maximum principal stress direction. It was observed that over a field of uniform stress state, the level of damage was also uniform, demonstrating the continuum behavior of damage.[8]

  Creep rupture is estimated by calculating creep rupture stress. Rupture stress is the stress a which damage reaches the maximum value i.e. $\omega = 0.99$. It is calculated using the utility subroutine which updates the value of rupture stress based on maximum principal stress at each integration point for every time step.

2.4 Isotropic Creep Damage Models

Creep is one of the major failures occurring in turbomachinery parts like turbine blades. It is a time-dependent deformation that occurs in metals when subjected to stresses at an elevated temperature, 0.4 times the absolute melting temperature of the material.[7] The analytical approach to accurately determine creep rupture life, is to simulate the primary and secondary creep response. Norton-Bailey model, which contains three temperature dependent regression constants can be used to predict creep strain behavior. By performing curve fitting to best fit the test data, creep constants can be determined and used to predict creep rupture life.[28]

To simulate the secondary and tertiary behavior of the creep curve, Continuum Damage Mechanics (CDM) based damage rate equations can provide accumulated damage, residual life, and rupture life prediction for a given stress.[16] Continuum Damage Mechanics (CDM) has provided a fundamental step toward accommodation of creep damage in final rupture of the specimen and prediction of full creep behavior. By using a damage parameter, time to rupture can be predicted accurately.[29]

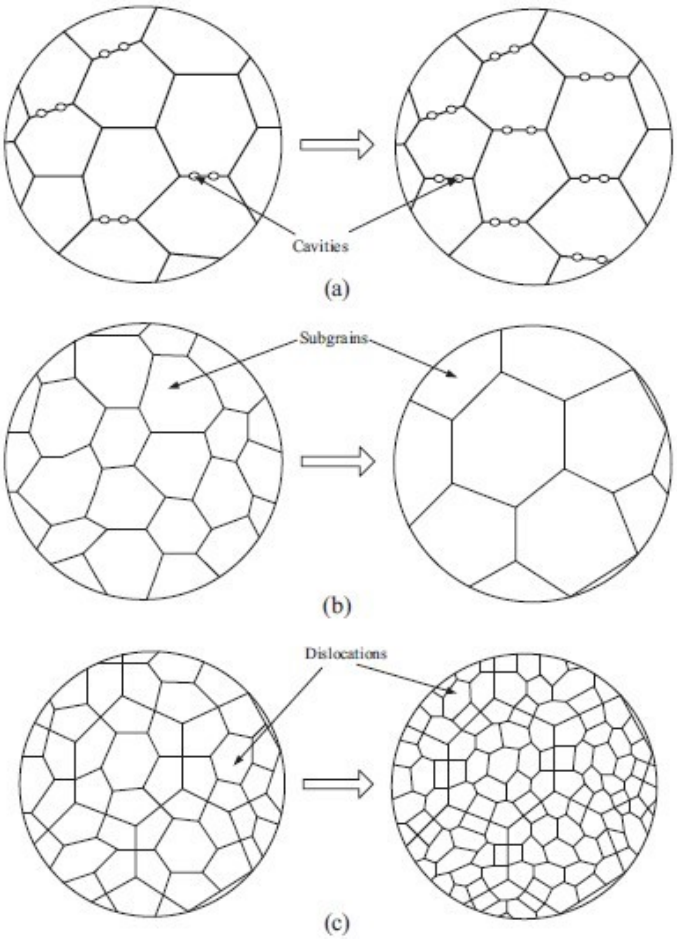

Figure 2.8. Schematic of microscopic damage mechanisms in the creep process: (a) nucleation and growth of grain boundary cavities, (b) dynamic coarsening of the sub-grain microstructure, (c) multiplication of the mobile dislocation density.[17]

Damage based creep constitutive equations are capable of fully considering of all three stages of creep associated with material deterioration.[7] In this section several isotropic creed damage models are discussed with a focus on single damage parameter models.

2.4.1 Kachanov-Rabotnov Damage Model

Creep damage evolution can be studied by incorporating the tertiary stage of creep deformation. The creep damage model originally proposed by Kachanov and Rabotnov is reasonably accurate in predicting the tertiary creep behavior of materials.[17] [25] [23] This phenomenological formulation has the creep rate and damage evolution defined as

$$\dot{\varepsilon}_{cr} = \frac{d\varepsilon_{cr}}{dt} = A\Big(\frac{\sigma}{1-\omega}\Big)^{n} t^{m} \tag{2.6}$$

$$\dot{\omega} = \frac{d\omega}{dt} = B\frac{\sigma^{\chi}}{(1-\omega)^{\phi}} \tag{2.7}$$

where the creep strain rate is similar to Norton's power law for secondary, 2.4, with the same associated A and n constants, σ is von Mises stress, and B, χ, and ϕ are tertiary creep damage constants.

The multiaxial form of this model is as follows.[17]

$$\dot{\varepsilon}_{\mathrm{ij}}^{cr} = \frac{3}{2}A\Big(\frac{\sigma_{eq}}{1-\omega}\Big)^{n} t^{m}\Big(\frac{S_{\mathrm{ij}}}{\sigma_{eq}}\Big) \tag{2.8}$$

$$\dot{\omega} = B\frac{\sigma_{eq}^{\chi}}{(1-\omega)^{\phi}} \tag{2.9}$$

and

$$\sigma_{rup} = \alpha\sigma_1 + (1-\alpha)\sigma_{eq} \tag{2.10}$$

where α is the material constant, which describes the effect of the multi-axial stress state behavior of material and ranges from $\alpha = 0$ (equivalent stress dominant) to $\alpha = 1$ (maximum principal stress dominant).The initial value of damage parameter is zero, representing the case with no damage.[28] As creep occurs, the damage variable increases until it reaches unity. If m is zero in 2.6, i.e., primary creep is considered negligible, it simplifies to

$$\dot{\varepsilon}_{cr} = A\Big(\frac{\sigma}{1-\omega}\Big)^{n} \tag{2.11}$$

2.4.2 Liu-Murakami Damage Model

The damage evolution relies heavily on the stress field and the stress sensitivity of Kachanov-Rabotnov model is not reliable and significantly effects on the damage localization. To overcome this difficulty and to accurately predict the creep damage evolution, an alternative creep damage model was proposed by Liu and Murakami.[17] The multiaxial form of this model is as follows.

$$\dot{\varepsilon}_{\mathrm{ij}}^{cr} = \frac{3}{2} A \sigma_{eq}^{n-1} S_{\mathrm{ij}} exp\left[\frac{2(n+1)}{\pi\sqrt{1+\frac{3}{n}}}\left(\frac{\sigma_1}{\sigma_{eq}}\right)\omega^{3/2}\right] \tag{2.12}$$

$$\dot{\omega} = M\frac{[1-exp(-q_2)]}{q_2}\sigma_{rup}^{\chi} exp(q_2\omega) \tag{2.13}$$

Where the failure stress σ_{rup} has the same form as in Kachanov-Rabotnov model of 2.10. The material constants A, M, n, q and χ can be obtained by curve fitting to the uniaxial creep curves. The damage variable ω can be given by integrating the 2.13 from 0 to ω for the damage variable and from 0 to t_f for the time t, as follows.

$$\omega = -\frac{1}{q_2} ln\left(1 - \left[1 - exp(-q_2)\frac{t}{t_f}\right]\right) \tag{2.14}$$

where,

$$t_f = \frac{1}{M\sigma^{\chi}} \tag{2.15}$$

L-M model is unique as it incorporates the damage variable in the rate equations in an exponential form. To include rupture, the applied stress can be replace with equivalent stress and the equations can be modified for rupture prediction calculations. Also the time to failure equation is used to calculate the predicted creep failure time.[17]

3. ISOTROPIC CREEP DAMAGE MODEL: FE USER DEFINED SUBROUTINE

3.1 Introduction

In all the general non-linear FEA software packages like ABAQUS and ANSYS, implementing tertiary creep and rupture require additional governing equations to be defined and solved for the integration points of the element at each time step. The built in models have the limitations of calculating the primary and secondary creep strain rate. Although, these packages have the ability to model the tertiary creep and rupture through user subroutines. User Subroutines are the extension of the FEA packages wherein the user can define their own governing equation to calculate or define parameters like Load, Element, Field, Material etc. and define the behavior (linear/non-linear) and integration schemes. Some examples of the user subroutines ABAQUS offers are:[9]

- **CREEP**: This subroutine is used to define the viscoplastic, time-dependent deformation in a material. The deformation is divided into deviatoric behavior (creep) and volumetric behavior (swelling).
- **DLOAD**: This subroutine is used to define nonuniform, distributed mechanical loads (pressures and body forces).
- **UEL**: This subroutine is used when it is necessary to create elements with an element formulation that is not available in ABAQUS/Standard.
- **UMAT**: This subroutine is used to define any complex, constitutive models for materials that cannot be modeled with the available ABAQUS material models.

For the current study, the CREEP subroutine is modeled to solve the classical isotropic Kachanov-Rabotnov model for tertiary creep damage. A rupture prediction model is incorporated in the Kachanov-Rabotnov model. Due to the limitations of damage prediction capabilities of the Kachanov-Rabotnov model the Liu-Murakami damage model is modeled using CREEP subroutine to compare the rupture and damage prediction capabilities of both the models.

Creep deformation and rupture experiments are simulated for samples of L-PBF Manufactured Nickel Alloy 718 (nickel based superalloy) tested at temperatures between 650°C under a 600 MPa load.[20] The creep constants used to simulate the creep response are calculated using regression curve fitting.

3.1.1 Constitutive Creep Model

To incorporate secondary and tertiary creep behavior, a constitutive model needs to be developed. Creep experiments show that for nickel based alloys, the primary creep regime is very short, and development of a primary creep model is not necessary as the primary region is very less in the experimental data. The primary regime is approximated by a static primary creep after loading the specimen.[25]

First, to account for steady state creep and tertiary creep several models were studied to select an adequate model to predict the alloy 718 behavior. A continuum damage mechanics (CDM) model involves the use of a damage variable which accounts for microstructural evolution.[22] Microcracks along the grain boundaries of polycrystalline materials cause stress concentration during the transition from secondary to tertiary creep. Due to the amplified stress a local reduction of cross sectional area occurs and sometimes vice versa. The damage variable is calculated on this phenomenological basis.[23] All the model used for this research are single damage parameter models. There are some models which incorporate more than one damage variable to account for a variety of physically observed damage mechanisms.[24] A continuous distribution of damage is an essential feature of a damage variable required for the application of a continuum damage mechanics model.

To define the creep mechanism numerically, it is important to define a relationship between the equivalent creep strain rate $\dot{\varepsilon}_{cr}$ and equivalent stress σ_{eq} of the form.

$$\dot{\varepsilon}_{cr} = f(\sigma_{eq}, T, t, \varepsilon, \omega_{\mathrm{i}}, ...) \tag{3.1}$$

Where T is temperature, t is time, ε is the strain, and $\omega_1,\ \omega_2, ..$ are the damage parameters. Using the flow rule [14] creep strain rate components can be obtained from $\dot{\varepsilon}_{cr}$

$$\dot{\varepsilon}_{\mathrm{ij}}^{cr} = \frac{3}{2}\dot{\varepsilon}_{cr}\frac{S_{\mathrm{ij}}}{\sigma_{\mathrm{eq}}} \tag{3.2}$$

In the K-R model if the value of $\omega = 0$ in equation 2.10, The tertiary creep damage model can be reverted back to secondary creep. Damage evolution becomes zero and the strain rate reverts back to the Norton power law for secondary creep.[23] This property has been exploited in a previous study to determine the transition time when the dominant creep regime shifts from secondary to tertiary creep.[25] This tertiary creep damage model has been used in a variety of studies of turbine and rotor materials. The constants A, n, M/B,χ, and ϕ/q_2 are considered material properties.

It is shown by Stewart and Gordon [25][22][24] that by determining the creep material constants at multiple temperatures for Ni-base alloy IN-617, temperature-dependent functions can be developed to model the tertiary creep damage. This makes the creep strain rate and damage evolution equations temperature dependent. As the temperature changes over time, the material constants change, which ultimately changes the creep strain rate and damage evolution predicted at the current time step.[25]

3.1.2 Rupture Prediction Model

A prediction of the rupture time can be achieved using the damage evolution equation 2.7. By separating the variables and integrating between the limits of $\omega_0 = 0$ and $\omega = 1$ for damage and $t_0 = 0$ to the time to fail t_f = t for time.[24] Integration of the equation leads to the following

$$(1-\omega)^{\phi}d\omega = B\sigma_{rup}^{\chi}dt \tag{3.3}$$

$$\frac{(1-\omega)^{\phi}}{(1+\phi)}\Bigg|_{\omega_0}^{\omega} = B\sigma_{rup}^{\chi}\Bigg|_{t_0}^{t} \tag{3.4}$$

Under creep experiment conditions, stress is constant and t_0 and ω_0 equal 0.0. Solving the integration leads to the rupture time and damage prediction equations:

$$t = [1 - (1 - \omega)^{\phi+1}][(\phi + 1)B\sigma_{rup}^{\chi}]^{-}1 \tag{3.5}$$

$$\omega(t) = 1 - [1 - (\phi + 1)B\sigma_{rup}^{\chi}t]^{1/(\phi+1)} \tag{3.6}$$

The sections below explain the implementation of the Kachanov-Rabotnov and Liu-Murakami CDM models in ABAQUS user subroutine using FORTRAN77.

3.2 Implementation of user subroutine USERCREEP

The isotropic creep damage models described in previous chapters have been implemented in ABAQUS using user subroutine CREEP in order to determine the creep curve for the additive manufactured nickel 718 alloy. The formulation was implemented into a FORTRAN routine in the form of a CREEP user subroutine in ABAQUS. The subroutine is incorporated with an implicit integration algorithm. This backward Euler integration algorithm is more accurate over long time periods than other practical numerical integration methods. This allows larger time steps that reduce the numerical solve time.[9] As mentioned in previous works done by Stewart and Gordon [25][22][24] , the viscoplastic/creep behavior of materials is significant at extended histories therefore, the backward Euler method is the desired method for integration of creep constitutive models.

An internal state variable is updated for every time step to store the required parameters. Initially, ω equals 0.0 and during loading, ω increases. The damage ω is restricted to a maximum of 0.99 to prevent the singularity that is caused by rupture (e.g., ω equals 1.0). To reduce the computation time, and large deformation errors, the subroutine was skipped for a general time step ($\omega = 0$) and Norton formulation was used. Also, the simulation was terminated once the total strain reached 100%. If needed, this model can be applied with time-dependent plasticity models in a straightforward manner.

3.2.1 K-R model USERCREEP subroutine

For simulating the creep response of 3D printed IN718 samples, based on the Kachanov-Rabotnov creep damage model, a creep subroutine defining the creep behavior according to the damage evolution equations as stated in Chapter 2.4.1 is modeled using FORTRAN. A flow chart of the implementation is shown in Figure 3.1 Since implicit integration is more effective when the response period is long relative to typical relaxation times, the subroutine is performed using backward Euler integration scheme.

All the creep strain rate and damage evolution equations are solved at each time step. At the start of a new increment, subroutine is called once for each integration point and estimated creep strain is calculated and stored based on the state of the start of the time increment. The subroutine is called multiple times and the nonlinear constitutive equations are solved using a local iteration procedure. The exact number of calls depend on the local iteration procedure. Stress is assumed constant during the time increment to calculate the equivalent creep increments.[23]

The Uniaxial equivalent deviatoric creep strain increment equation 2.6 is partially differentiated with respect to applied stress.

$$\frac{\partial \Delta \dot{\varepsilon}_{cr}}{\partial \tilde{\sigma}} = An\Big(\frac{\sigma}{1-\omega}\Big)^{n} t^{m} \tag{3.7}$$

In order to calculate the creep strain, increment as per the Equation 3.7 the value of ω is needed at each time step per integration point. For that purpose, an iterative damage evolution update equation is added in the code with limits $\omega_0 = 0$ till $\omega = 0.99$. The maximum value of ω is limited to 0.99 to avoid singularity.

$$\omega = \omega + \Delta\omega \tag{3.8}$$

The testing curves show a very small primary creep region. To avoid calculating the primary creep strain response, in Equation 3.7 the value of m = 0 considers only the secondary and tertiary region of the creep curve. The rupture stress (σ_{rup}) is equal to the applied uniaxial stress ($\tilde{\sigma}$) for a uniaxial stress situation.

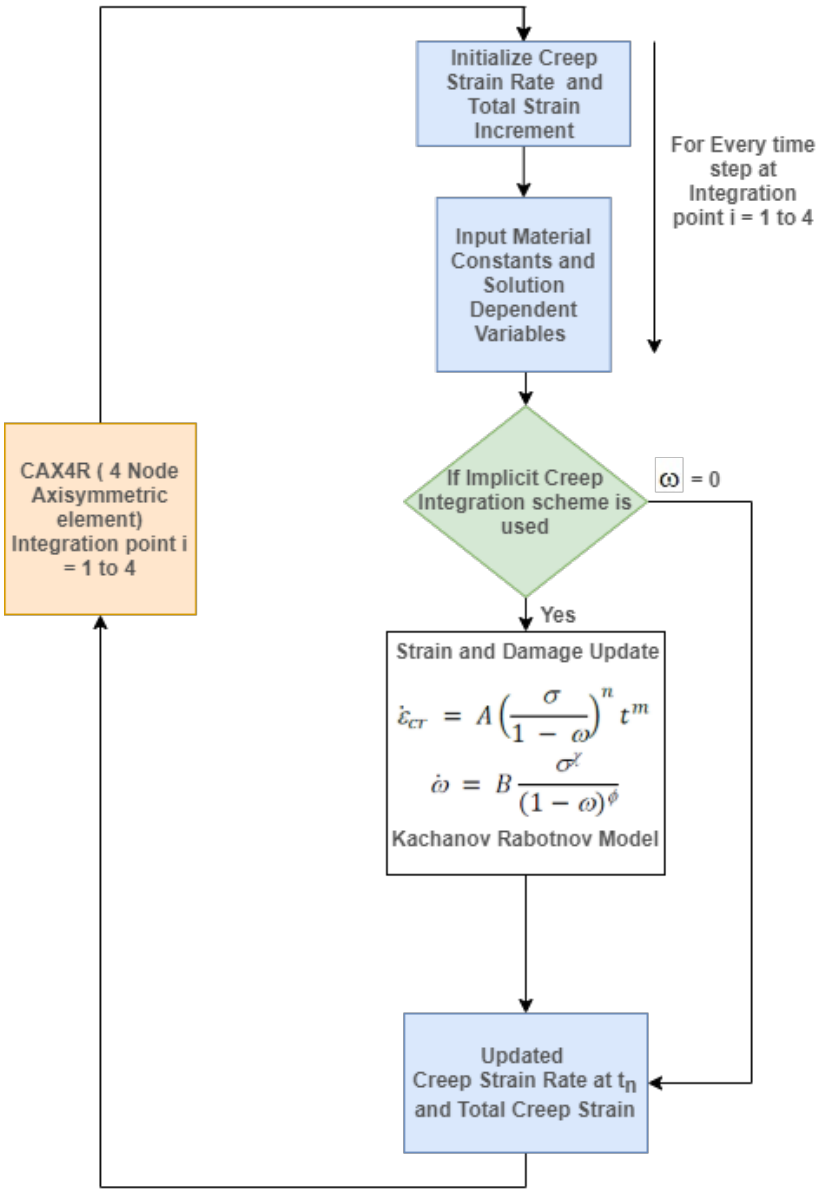

Figure 3.1. Flowchart on the Kachanov-Rabotnov model implementation.

3.2.2 K-R model limitations

In the K-R model amplified stress due to a local reduction in cross-sectional area is the basis of the damage variable, ω. In CDM, damage ω, is assumed to be homogeneous and irreversible. In the K-R model, the damage calculation is performed only in the tertiary creep stage and no damage is updated in primary and secondary creep stages.[5]

For damage to be unity at failure, instantaneous strain ($\dot{\varepsilon}_{cr}$) has to be infinitely large, which cannot be true, and creep strain rate becomes large just before failure and remains finite throughout the lifetime. Therefore, KR model damage remains very low up to 90% of lifetime.[5] The instantaneous strain ($\dot{\varepsilon}_{cr}$) varies from 0.2-0.8 for most metals

Rearranging Equation 2.11

$$\omega(\dot{\varepsilon}_{cr}) = \frac{\left(\frac{\dot{\varepsilon}_{cr}}{A}\right)^{1/n} - \sigma}{\left(\frac{\dot{\varepsilon}_{cr}}{A}\right)^{1/n}} \tag{3.9}$$

From Equation 2.7, as mentioned by when $\omega = 1$, $\dot{\omega}$ increases exponentially. It attempts to sum up both the continuous damage of creep and discontinuous plastic damage that occurs at the instant of fracture. The damage calculation is performed only in the tertiary creep stage leading to an exponential increase in damage and hence creep strain.[5] Thus, needing a better approach to overcome this issue.

3.2.3 K-R model with rupture prediction

To model the creep rupture, based on the creep rupture time equation, the rupture stress is calculated using the Equation 3.5 and 3.6 and is implemented in the creep subroutine through user defined field (USDFLD). In the equation σ_{rup} is the failure stress which is assumed to be a function of the maximum principal stress σ_1 and the equivalent stress σ_{eq}, as shown in Equation 2.10.

- **USDFLD**: User defined field. When complex material behavior needs to be modeled and the user does not want to develop a UMAT subroutine, USDFLD is used. Field variables can be redefined at material (integration) points of an element by USDFLD.[9] It allows the user to define f_{i} (functions of field variables) at every integration point of an element. The subroutine has access to solution data like stress, strain, plastic strain, principal stress etc. To simulate rupture, using the ABAQUS utility routine GETVRM, we get the value of maximum principal stress at the given integration point of the element.[9]

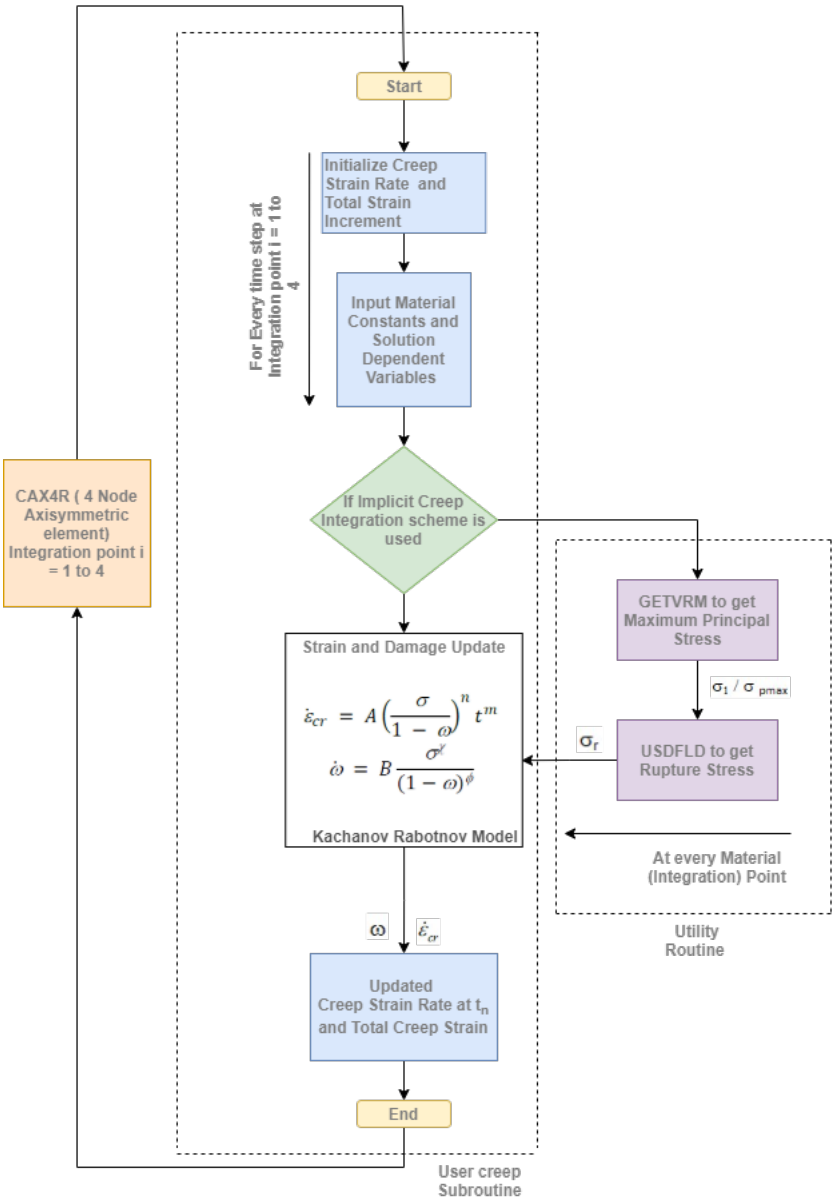

Figure 3.2. Flowchart on the Kachanov-Rabotnov model with Rupture implementation.

To create field-variable-dependent material properties two methods can be used, (a) Using tabular definition for built-in ABAQUS material models, (b) Using other user subroutines, such as CREEP, to define the material behavior as a function of f_i. For most nonlinear material behavior (i.e., plasticity) ABAQUS/Standard uses an implicit integration method to calculate the material behavior at the end of the current increment.

- **GETVRM**: Material point information. The subroutine GETVRM provides USDFLD with access to the solution data stored in databases during the analysis. For storing the value of maximum principal stress at each integration point, the CALL GETVRM('SP') command is issued.[9]

```
 CALL GETVRM('SP',ARRAY,JARRAY,FLGRAY,JRCD,JMAC,JMATYP,
1 MATLAYO,LACCFLA)

 STATEV(2) = ( ABS( ARRAY(3) )+ ARRAY(3) ) / 2
```

Figure 3.3. Extracting maximum principal stress.

Double index components (tensors) are returned in the order 11, 22, 33, 12, 13, 23 for symmetric tensors, followed by 21, 31, 32 for asymmetric tensors, such as the deformation gradient. [28] Thus, the stresses for a plane stress element are returned as ARRAY(1) = S11, ARRAY(2) = S22, ARRAY(3) = 0.0, and ARRAY(4) = S12. Three values are always returned for principal value requests, the minimum value first and maximum value third, regardless of the dimensionality of the analysis.[9]

The order in which the subroutines within the .for file are called is extremely important. The USDFLD subroutine needed to be called prior to the creep subroutine. Using GETVRM maximum principal stress is calculated at the material (integration) points. To incorporate error in calculations, JRCD command is used in an IF statement. JRCD stores the return code (0 = no error and 1 = output request error or all components of output request are zero). A flowchart is shown below to represent the implementation of Kachanov-Rabotnov model incorporating the rupture stress.[9] To calculate the rupture stress using Equation 2.10 the value of maximum principal stress is fed into the equation for rupture stress and the damage evolution equation.

3.2.4 L-M model USERCREEP subroutine

The ill-natured stress sensitivity of Kachanov-Rabotnov creep model has significant effects on the damage localization as the damage evolution is closely linked with the stress field. An alternative creep damage model was proposed by Liu and Murakami to eliminate this difficulty and accurately predict the creep damage evolution.[17] It demonstrated that creep deformation in all three stages as well as creep rupture time can be accurately predicted using the creep damage model.[19] The uniaxial form of Liu Murakami damage model is defined as follows.

$$\dot{\varepsilon}_{cr} = \frac{3}{2} A \sigma_{eq}^{n} exp \left[\frac{2(n+1)}{\pi \sqrt{1+\frac{3}{n}}} \omega^{3/2} \right] \tag{3.10}$$

and the uniaxial form of damage equation is.

$$\dot{\omega} = M \frac{[1 - exp(-q_2)]}{q_2} \sigma_{rup}^{\chi} exp(q_2 \omega) \tag{3.11}$$

where, A, M, n, q_2 and χ are the material and damage constants. The limitations faced by Kachanov-Rabotnov model of stress-sensitivity and mesh dependence can be mitigated by representing damage as an exponential function within the creep rate and damage evolution equations.[6]

Using the utility subroutine explained in earlier section the value of rupture stress is fed in the Liu Murakami damage evolution Equation 3.11 The subroutine performs similar to the previously explained routines, the difference is the governing equation to calculate creep strain rate and the material constants for the Liu Murakami model.[19] The flow chart is given below.

The governing equation impact the creep strain rate calculations. The models described above are implemented for stainless steel and nickel based alloys for validation with test data.

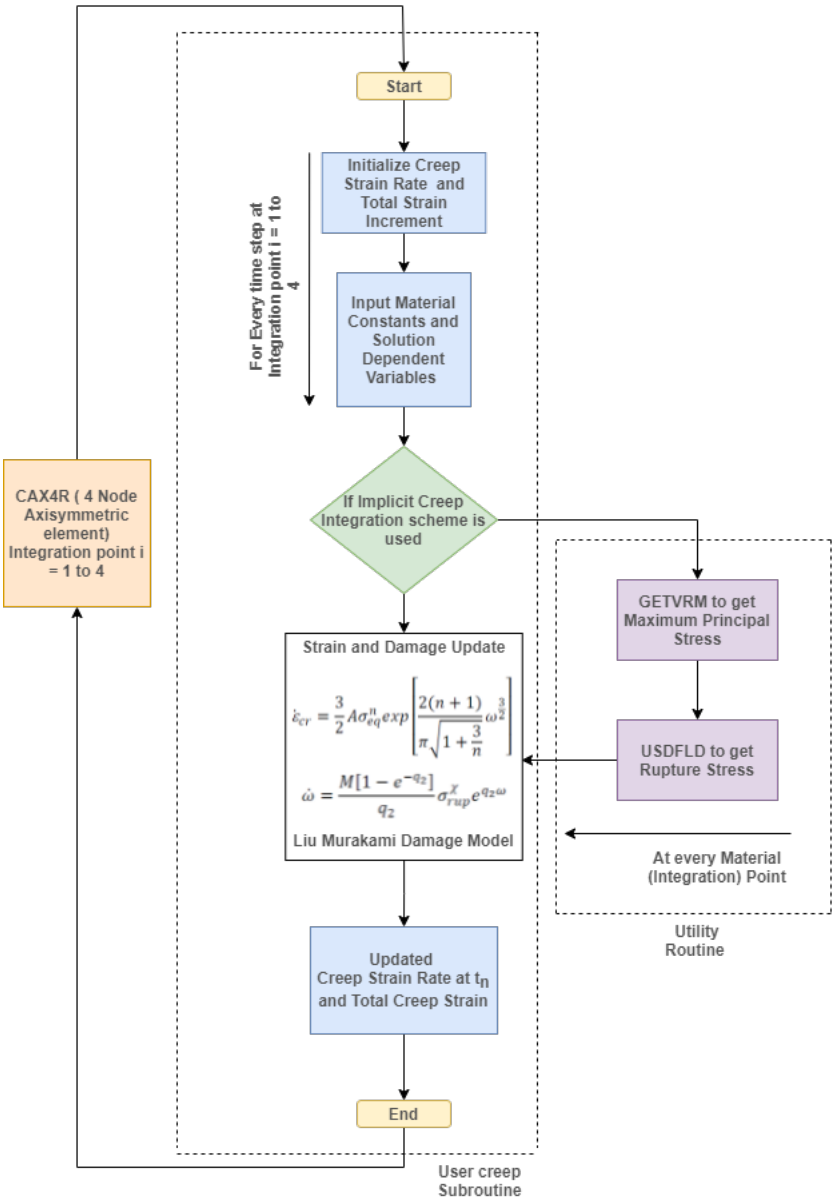

Figure 3.4. Flowchart of the Liu-Murakami model with Rupture implementation.

3.3 Single Element Testing

The subroutines are used to simulate the temperature and stress loading conditions of a series of uniaxial creep and rupture experiments for Stainless steel 316 and Nickel Alloy 718. We first investigate a single element test, given in Fig . The dimension of a 2D shell element is 10mm x 10mm.[25]

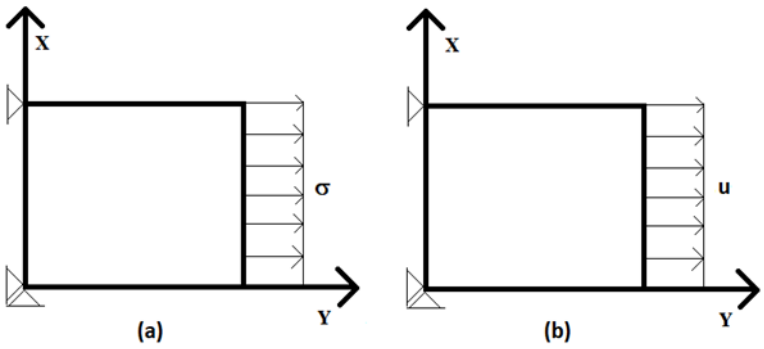

Figure 3.5. Single element test problem set up (a) creep loading and (b) constant displacement loading.

The single element tests were done for the reduced integration plane strain elements with linear and quadratic interpolation schemes (CPE4R and CPE8R in ABAQUS). The elements were tested for response under constant load (creep) and constant displacement (relaxation) boundary conditions. The material parameters were used as stated in the creep constant determination chapter previously.

3.3.1 K-R model comparison with rupture implementation

A comparison of K-R model to calculate the damage evolution behavior is done for model with and without rupture implementation. It was found out that the K-R model without rupture predicts the damage more aggressively towards the end i.e., as the damage reaches its maximum value. Damage evolution is defined as the rate of change of damage with respect to the time to failure. For stainless steel 316, a comparison of the damage rate prediction capability of the Kachanov Rabotnov usercreep, with and without rupture, were observed. The element was subjected to 260 MPa and K-R models were compared for the creep constants calculated at 600°C.

The model which incorporates rupture stress shows a gradual increase in damage and the time to failure is 645.5 hours. Whereas the model without rupture , increases damage exponentially to 0.99 towards the end. The time to failure.is 1066.5 hours which is almost double.

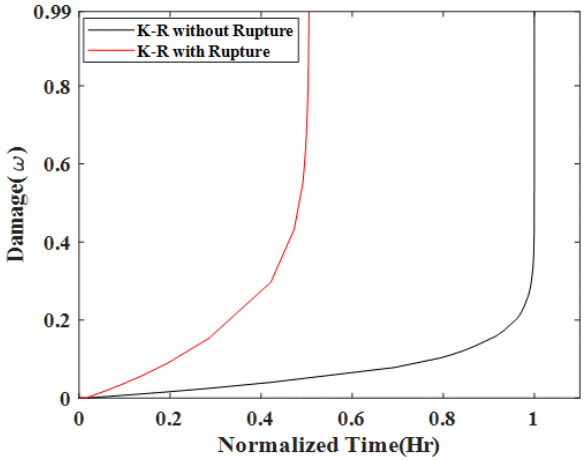

Figure 3.6. Damage evolution plot: damage vs normalized time plot for K-R model with and without rupture implementation.

As per Equation 2.10 the value of rupture stress calculated by the utility subroutine correctly estimates the damage rate ($\dot{\omega}$) value for each time step and is able to predict damage correctly along with the rupture time.

As we can see in the damage Equation 2.7 , the rate of damage ($\dot{\omega}$) depends on ϕ which is the damage variable. The value of ϕ is selected such that best fit is obtained for the creep strain curve when compared to the experimental data. A series of single element tests were performed for stainless steel 316 creep constants to monitor the effect of on the damage evolution for the K-R model with rupture. Based on various literature, the value of ϕ for 316 steel was found to be 7 for a good fit. Using K-R constants for stainless steel 316 at 600°C and 260MPa, single element tests are performed by varying ϕ (5,7,9,13).

It can be observed that as ϕ increases, the damage behavior becomes steeper. For a higher value of ϕ the damage is exponential as rupture approaches and a sudden increase in damage is observed. Whereas for a lower value of ϕ the damage is more gradual and less sudden towards rupture. As observed, here a large value of ϕ implies very large stress sensitivity of the damage evolution.

A similar behavior is observed with the creep strain calculations. For lower value of ϕ the creep strain rate is lower as compared to the higher values of ϕ.

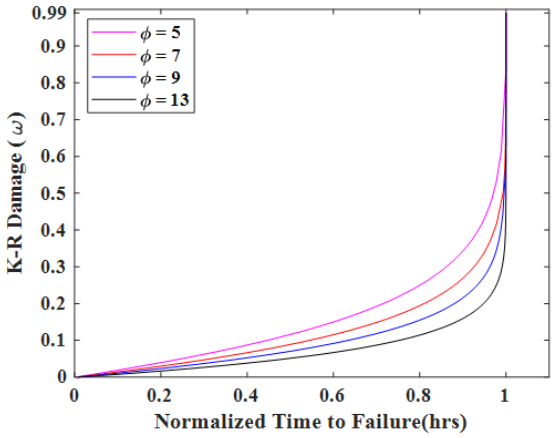

Figure 3.7. K-R damage vs normalized time to failure ($0 < \omega < 0.99$) for $\phi = 5, 7, 9, 13$ with time to failure = 645.5 hours.

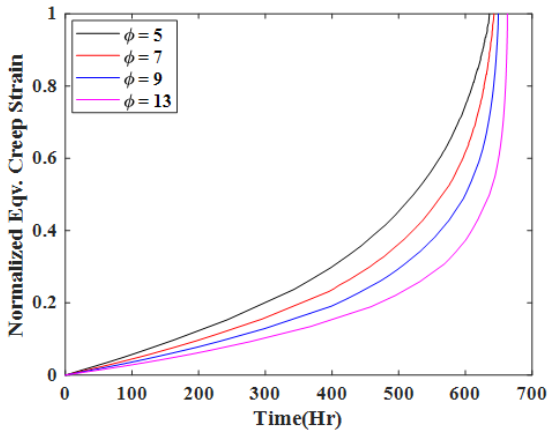

Figure 3.8. K-R model with rupture: Normalized creep strain vs Time for ϕ = 5,7,9,13.

3.3.2 Damage evolution: K-R vs L-M model

Similar single element tests were performed for 316 steel to compare the damage evolution and creep strain rate prediction capability for the L-M model.

The feature of K-R damage evolution is that, though the damage remains quite small value throughout the early stage, the damage development has a steep acceleration at the final stage of lifetime. This feature becomes more noticeable when compared to L-M model. Here we can see that the stress sensitivity is not observed with the damage evolution curve for L-M model.

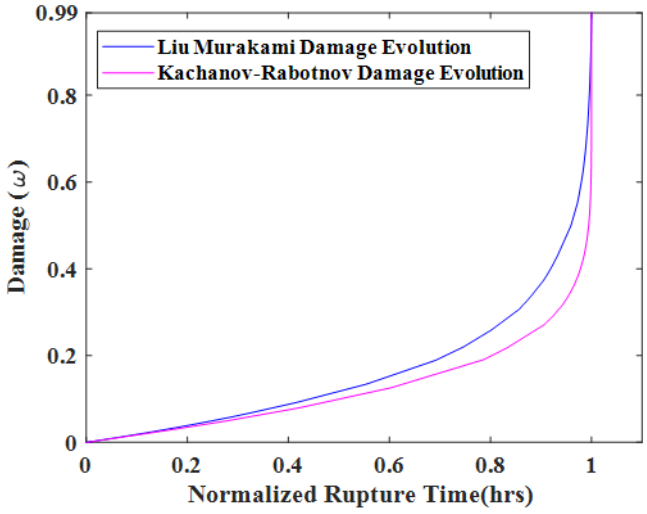

Figure 3.9. Damage evolution plot: damage vs normalized rupture time plot for K-R vs L-M model.

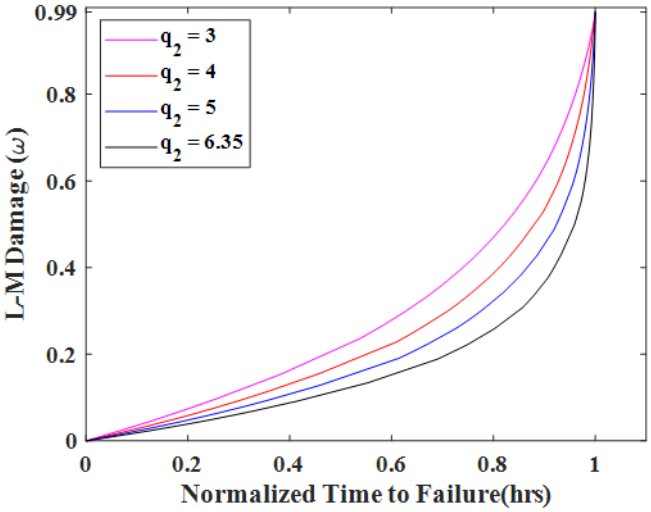

Figure 3.10. L-M damage vs normalized time to failure ($0 < \omega < 0.99$) for q_2 = 3,4,5,6.35 with time to failure = 663.156 hours.

The damage variable for L-M model is q_2 and as per Equation 2.13, it has a similar impact on damage and creep prediction. A similar trend is observed with the L-M model when the damage and creep strain are plotted for varying q_2.

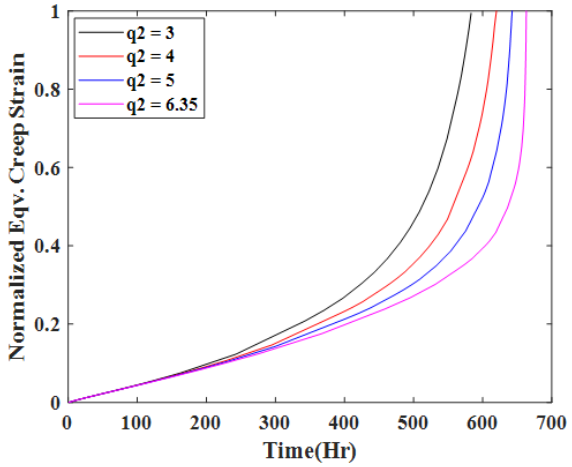

Figure 3.11. L-M model: Normalized creep strain vs Time for q_2 = 3,4,5,6.35.

3.3.3 Stress and temperature dependence

Creep strain rate is majorly dependent of temperature and stress. As per Equation 3.1 we can see that creep strain is a function of stress, temperature, and damage. For accurate creep strain prediction capability, the CDM are tested for their sensitivity towards stress and temperature.

For the L-M model, single element tests were performed for two different materials. Stainless steel 316 stress dependent constants were used calculated at 600°C for a stress range of 240-300 MPa and nickel alloy 718 temperature dependent constants were used calculated at 650, 704, and 760°C for a constant applied stress of 551 MPa.

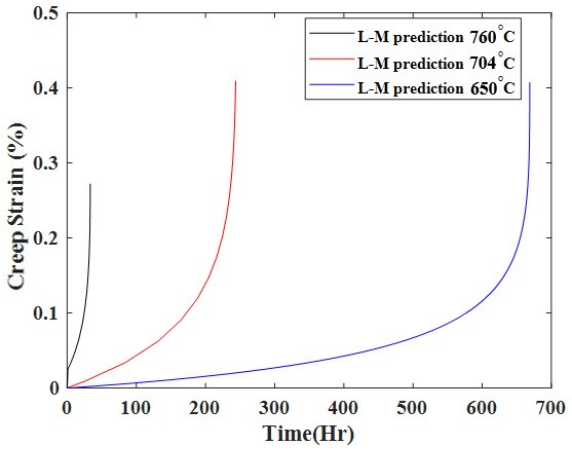

Figure 3.12. L-M model: Temperature dependence for nickel alloy 718.

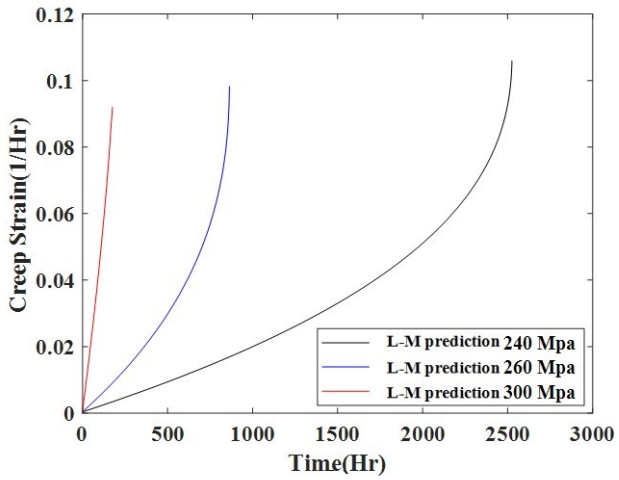

Figure 3.13. L-M model: Stress dependence for stainless steel 316.

The L-M model shows agreement with the creep prediction nature as we can clearly see how with an increase in stress and temperature, creep strain rate is increasing and time to failure is increasing.

3.4 User subroutine validation

To validate the CDM models, it is necessary to compare the creep strain predictions to the experimental data. The L-M model is used to simulate creep strain curves for stainless steel 316 and nickel alloy 718. Using the uniaxial creep data, the predictions are validated against the test data.

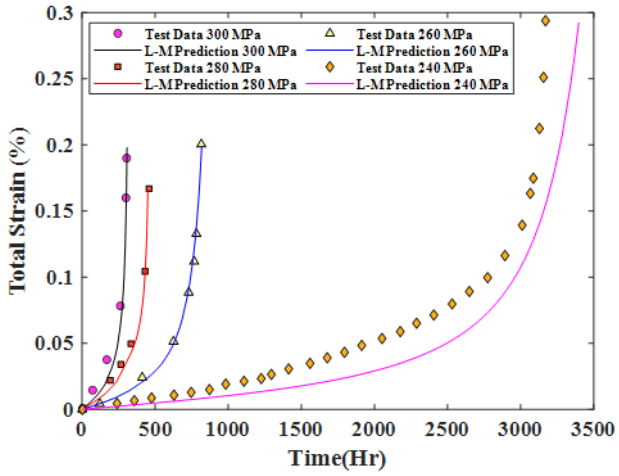

Figure 3.14. Uniaxial creep validation with experimental data for stainless steel 316 at 600°C for stress range 240 – 300 MPa.[28]

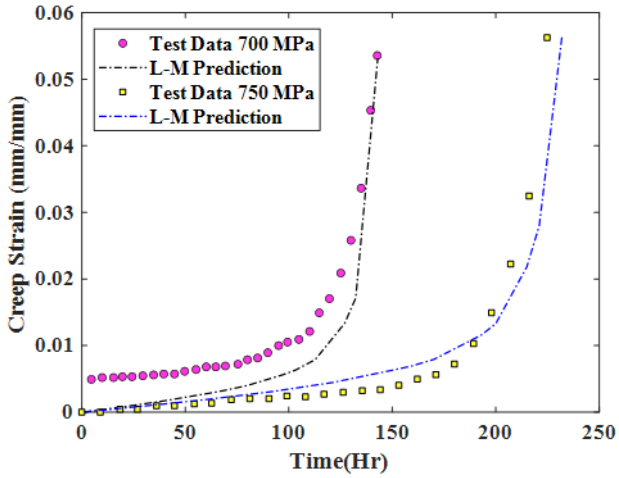

Figure 3.15. Uniaxial creep validation with experimental data for nickel alloy 718 at 650 °C and stress condition of 700 750 MPa.[26]

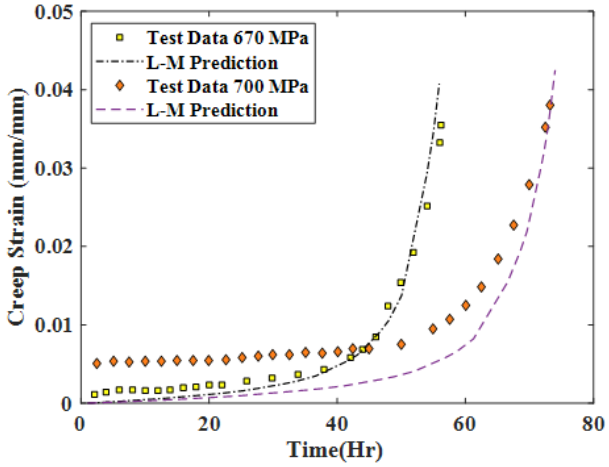

Figure 3.16. Uniaxial creep validation with experimental data for nickel alloy 718 at 675 °C and stress condition of 670 700 MPa.[26]

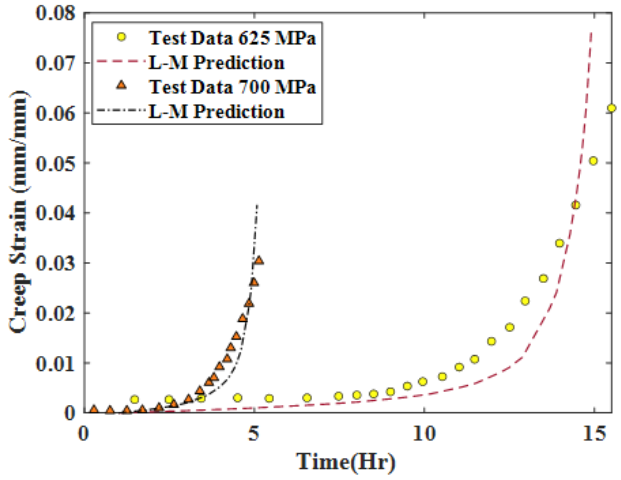

Figure 3.17. Uniaxial creep validation with experimental data for nickel alloy 718 at 700 °C and stress condition of 625 700 MPa.[26]

A single element test FEM setup is used, and test accurate stress is applied to calculate total strain vs time plots. It can be observed that the model is able to predict high stress regions of the creep curve accurately. For the lower stress, the model seems to over predict the strain. The values of q_2 and α are calculated to achieve the best fit. For nickel alloy 718, temperature dependent creep test data is used for validation of the L-M model. A good agreement is seen between the test and prediction data.

4. PROPERTY PARAMETERS USED IN CREEP MODEL

4.1 Introduction

Long term creep data is available mostly for general materials. There exists a shortage of creep data available for unconventional materials. When it comes to long term creep testing i.e. monitoring creep rupture for thousands of hours, data sparsity can be seen for most metals. For the different manufacturing processes, like additive manufacturing where the grain boundaries are unique and different from traditional manufacturing, creep data is not always present in the short, intermediate, and long term regime or minimum creep strain rate, stress rupture, etc. form.[4]

To get more reliable extrapolations, it is hypothesized that any form of creep data can by cross-calibrated using a constitutive model. A CDM constitutive model with coupled creep strain rate and damage equations enables calibration using desperate creep data. It is capable of predicting minimum creep strain rate, deformation, stress rupture, and damage using a single set of differential equation.[6]

This chapter includes all the material properties used for the FE modeling. The FE simulations were modeled using the elastic-plastic-creep material properties for stainless steel 316, wrought alloy 718 and additive manufactured nickel alloy 718. Two creep damage constitutive models of Kachanov-Rabotnov and Liu-Murakami were adopted, and corresponding material parameters were determined.

4.2 Mechanical Properties: Additive Manufactured Nickel Alloy 718

Nickel alloy 718 is a precipitation-strengthened Ni–Cr–Fe– Nb based superalloy. It exhibits very high yield and ultimate tensile strengths, high creep rupture strength, high fatigue strength and corrosion resistance, for extended times, at temperatures up to 620°C.[10] For the same reason, nickel alloy 718 is often used to fabricate aeroengine structures, turbines, liquid fuels rockets, rings, casings, cryogenic tanks, and various other high temperature applications. It is known to have good tensile, fatigue, creep, and rupture strength. A typical composition limits are shown in Table.

Table 4.1. Limiting chemical composition.[1]

Element	Composition
Nickel (plus Cobalt)	50.00-55.00
Chromium	17.00-21.00
Iron	Balance*
Niobium (plus Tantalum)	4.75-5.50
Molybdenum	2.80-3.30
Titanium	0.65-1.15
Aluminum	0.20-0.80
Cobalt	1.00 max.
Carbon	0.08 max.
Manganese	0.35 max.
Silicon	0.35 max.
Phosphorus	0.015 max.
Sulfur	0.015 max.
Boron	0.006 max.
Copper	0.30 max.

For additive manufactured nickel alloy 718, the mechanical properties are found to be superior to the traditionally manufactured counterparts. Yanjin Lu[15] performed a series of tensile tests on SLM manufactured nickel alloy 718 at initial strain rate of 2mm/s. the typical stress-strain curve for the nickel alloy is shown in Figure 4.1.Tensile properties which were calculated are shown in Table 4.3 and are used in modeling the elasto-plastic behavior for the FEM simulation.

Table 4.2. Temperature dependent mechanical properties of nickel alloy 718.[19]

Temperature ($°C$)	Youngs Modulus (GPa)	Poisson's Ratio	Yield Strength (MPa)
20	205	0.295	1161
200	190	0.28	1083
400	178	0.272	1036
620	166	0.279	992
700	159	0.291	878

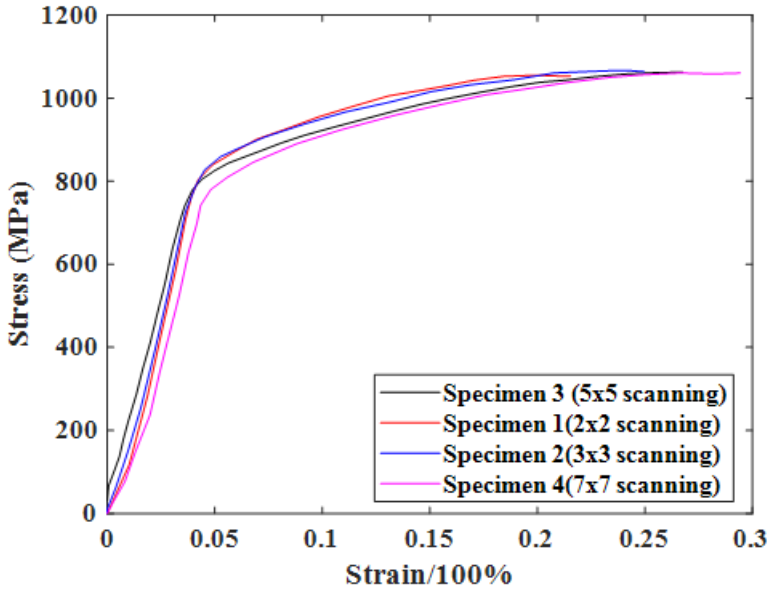

Figure 4.1. Stress vs Strain plots for different scanning size manufactured specimen AM 718. [15]

Table 4.3. Mechanical properties obtained from stress strain curve.[15]

Specimen	Yield Strength (MPa)	Ultimate Strength (MPa)	Elongation(%)
1 (2x2)	804±49.5	1076.5±28.9	16.85±0.07
2 (3x3)	800.5±7.80	1075.0±8.50	21.05±0.21
3 (5x5)	770.5±2.10	1064.5±3.50	22.35±0.21
4 (7x7)	772.5±2.20	1065.0±1.40	25.25±0.35

The creep simulation is performed for two different build orientations for the additive manufactured nickel 718. Sanches[20] performed uniaxial creep tests on cylindrical specimen. Three different build orientations were used for the manufacturing of AM 718 specimen as shown in Figure 4.2

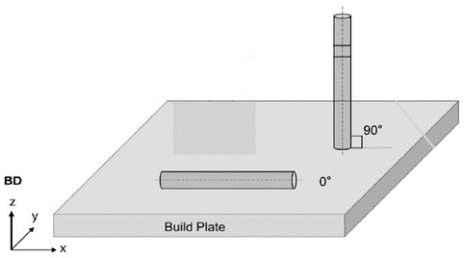

Figure 4.2. Build orientation for additive manufactured samples.[20]

A similar experimentation was performed by Reinshaw[1] for the XY and Z build orientations. Mechanical properties for a layer thickness of 30 m were calculated according to the standards.

Table 4.4. Mechanical properties for XY(0°) and Z(90°) build orientation.[1]

Specimen	Ultimate Tensile Strength (MPa)	Yield Strength (MPa)	Elongation(%)	Youngs Modulus (GPa)
XY(As Built)	1040	758	30	186
Z(As Built)	971	636	36	158
XY(Solution treated)	1467	1259	17	195
Z(Solution treated)	1391	1202	17	186
XY(HIP treated)	1379	1088	25	207
Z(HIP treated)	1346	1088	24	201

Properties shown in 4.4 are used to model the elasto-plastic behavior of additive manufactured 718 alloy for the creep test.

4.3 CDM creep parameter estimation

A creep test is used to determine the amount of deformation a material experiences over time while under a continuous tensile or compressive load at a constant temperature. Creep tests are fundamental for materials that are needed to withstand certain operation temperatures under load. For materials such as metals or alloys, their material properties change significantly at higher or lower temperatures.[11] A constant load is applied to a creep specimen while maintaining a high temperature environment. Strain gauges are attached to the gauge of the creep specimen to measure the total strain. While testing, the material's deformation is recorded at specific time intervals and overall data is plotted on a creep vs time diagram. The slope at any point on this curve is known as the creep rate, in which units are expressed in terms of in/in/hr or percent(%) elongation/hr. [11]

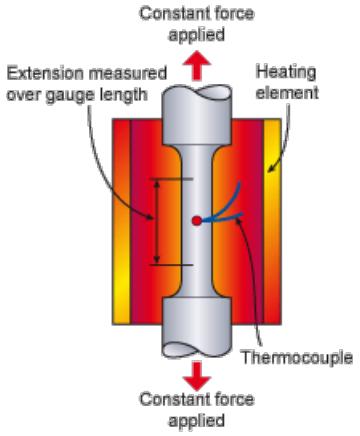

Figure 4.3. Schematics of a creep test.[14]

Testing is generally carried out in air at atmospheric pressure. However, if it is necessary to produce creep data for materials that react with air these may be tested in a chamber containing an inert atmosphere such as argon or in a vacuum.[14]

4.3.1 Creep constant estimation

To simulate creep failure using CDM, it is important to accurately estimate the material and damage constants. Here we have two CDM models, the K-R and L-M model with a set of material and damage constants embedded into the governing equations.

4.3.2 K-R model constants

In order to obtain initial estimates for the A and n values, the initial stages of creep data, for which $\omega = 0$ is used. Taking log on both sides for Equation 2.4

$$\dot{\varepsilon}_{cr} = A\sigma^n \tag{4.1}$$

$$log(\dot{\varepsilon}_{cr}) = -nlog(\sigma) + log(A) \tag{4.2}$$

The constants A and n can be estimated by plotting $log(\dot{\varepsilon}_{cr})$ versus $log(\sigma)$ and using a straight line fit to the data, as described in Figure 4.4

In order to determine initial values of B and χ and ϕ , Equation 2.7 is integrated and taking log on both sides gives

$$t_f = \frac{1}{B(\phi+1)\sigma^{\chi}} \tag{4.3}$$

$$log(t_f) = -\chi log(\sigma) + log\left(\frac{1}{B(\phi+1)}\right) \tag{4.4}$$

Hence by plotting $log(t_f)$ versus $log(\sigma)$ using data obtained from experimental uniaxial creep tests, the χ and B values can be identified from the gradient and the y-intercept.

Using the data found in literature, Table 4.5 show creep constants for some commonly used metals. The value of ϕ and α are calculated using the single element tests to obtain the best fit with experimental data.

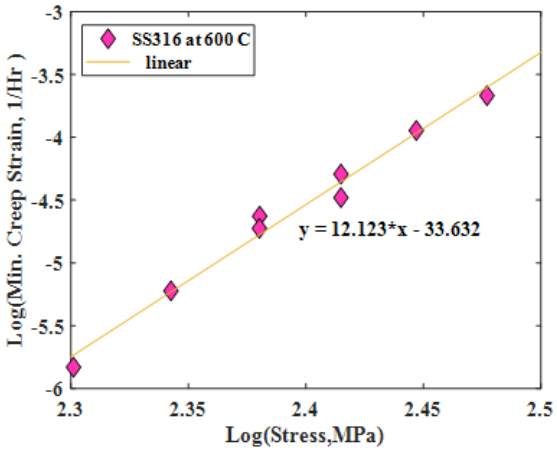

Figure 4.4. Log-Log plot to determine secondary creep constants for stainless steel 316 at 600 °C.

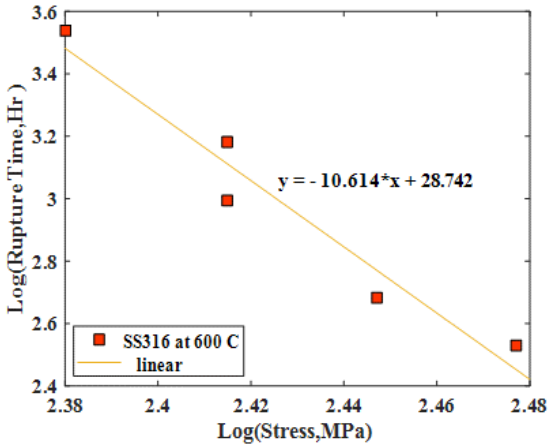

Figure 4.5. Log-Log plot to determine tertiary creep constants for stainless steel 316 at 600 °C.

Table 4.5. K-R creep constants for metals.[28]

Material	A ($MPa^{-n}hr^{-1}$)	n	B ($MPa^{-\chi}hr^{-1}$)	χ	ϕ	α
P91 at 650°C & 70-100 MPa	1.09E-20	8.462	2.95E-16	6.789	3.2	0.313
Waspalloy at 700°C & 520-750 MPa	2.35E-43	14	1.91E-41	13.490	13.0	0.150
Stainless Steel 316 at 600°C & 240-300 MPa	1.47E-29	10.147	1.88E-31	10.949	13.5	-
Stainless Steel 316 (Calculated) at 600°C & 240-300 MPa	2.344E-34	12.123	1.811E-29	10.614	7.0	-

4.3.3 L-M model constants

Similar to the K-R model, for ω=0 the creep strain rate equation is simplified to Equation 4.1 and a plot of $log(\dot{\varepsilon}_{cr})$ versus $log(\sigma)$ is used to determine A and n using a straight line fit to the test data.

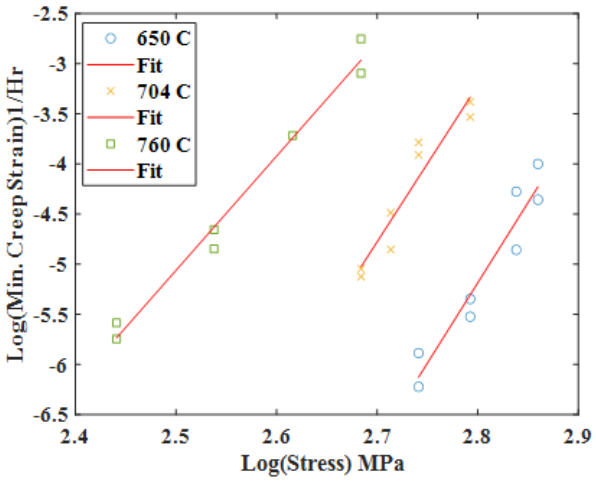

Figure 4.6. Log-Log plot to determine secondary creep constants for IN 718 alloy at 650, 704 and 760 °C.

The creep rupture data is used to determine the M, and χ tertiary creep constants for L-M model. The damage rate equation can be integrated and simplified to derive a time to failure equation.

$$t_f = \frac{\sigma^{-q_2}}{M} \tag{4.5}$$

This equation is similar to Equation 4.3 for K-R model. Thus, constants M and q_2 can be obtained using a straight line fir to a log-log plot similar to the tertiary creep constant determination in K-R model.

$$log(t_f) = -q_2 log(\sigma) + log\left(\frac{1}{M}\right) \tag{4.6}$$

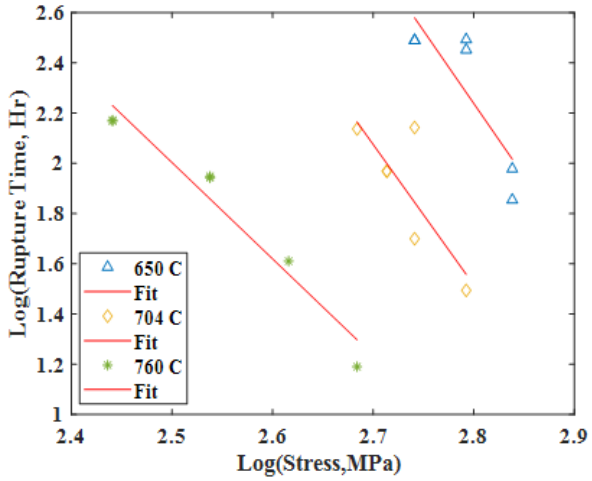

Figure 4.7. Log-Log plot to determine tertiary creep constants for IN 718 alloy at 650, 704 and 760 °C.

Table 4.6. L-M creep constants for nickel alloy 718.

Nickel alloy 718	A $(MPa^{-n}hr^{-1})$	n	M $(MPa^{-\chi}hr^{-1})$	χ	q_2	α
Reference[19] at 620°C	2.03 E-61	19.3	5.619 E-16	14.72	3.5	0.1
Calculated at 650°C & 551-724 MPa	4.75E-60	19.36	1.76E-28	9.15	5.0	0.478
Calculated at 704°C & 483-620 MPa	6.456E-47	15.363	2.41E-27	9.10	4.5	0.3
Calculated at 760°C & 413-483 MPa	6.58E-34	11.22	1.11E-12	3.98	3	0.2

L-M model constants for nickel alloy 718 creep test data are shown in Table 4.6. The constants given in the reference are calculated using a different calibration process and it can be seen that the calculated constants are in good agreement.

4.4 Additive manufactured nickel alloy 718

Creep test data for AM 718 is used to calibrate the K-R and L-M model and constants are determined using the approach mentioned in the previous section. The creep data for AM 718 is shown in the Figure 4.8.[20] Majorly for two build orientations i.e., XY and Z the creep strain rates are calculated. A clear difference is observed in the tertiary region for different specimen. During creep testing, the loads are applied in the axial directions and thus the Z build shows a better creep resistant as compared to the XY build.

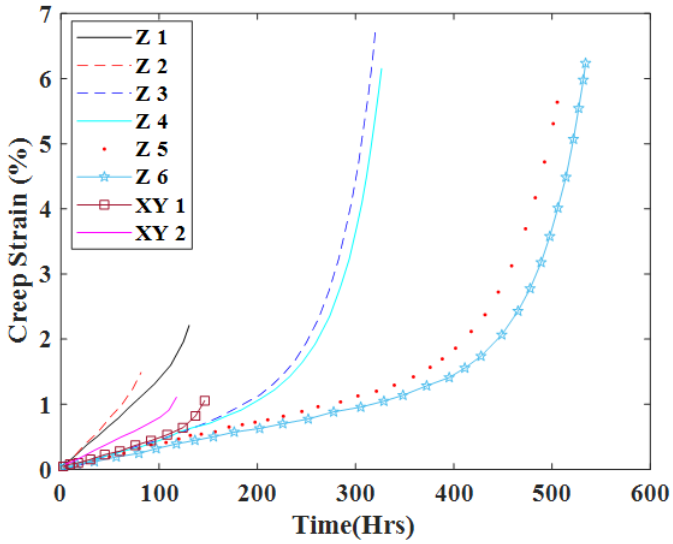

Figure 4.8. Creep curves for the different test cases, showing the clear differences in creep performance with regards to orientation. This also shows the differences in tertiary creep for the different specimens.[20]

4.4.1 Creep constant estimation

Based on the constant determination procedure mentioned for the L-M model, secondary creep and damage constants are calculated for AM 718.

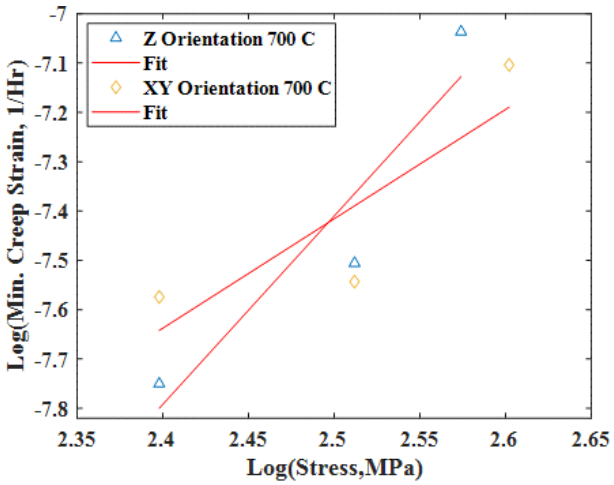

Figure 4.9. Log-Log fit: creep strain data for AM 718 at 700°C.

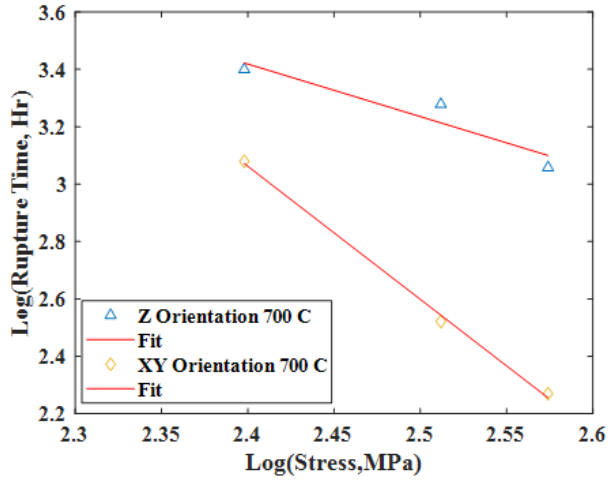

Figure 4.10. Log-Log fit: creep rupture data for AM 718 at 700°C.

The calculated constants are used to simulate the creep test using the L-M and K-R CDM model. The total strain versus time plots is compared with the experimental creep data. Nature of damage prediction is observed for both models.

Table 4.7. K-R creep constants for additive manufactured nickel alloy 718.

Orientation	A ($MPa^{-n}hr^{-1}$)	n	B ($MPa^{-\chi}hr^{-1}$)	χ	ϕ	α
XY at 700°C & 250-400 MPa	5.87489E-09	0.2738	1.47571E-15	4.9007	7	0.3
Z at 700°C & 250-375 MPa	2.32274E-12	1.6198	1.21619E-15	4.8023	5	0.1

Table 4.8. L-M creep constants for additive manufactured nickel alloy 718.

Orientation	A ($MPa^{-n}hr^{-1}$)	n	M ($MPa^{-\chi}hr^{-1}$)	χ	q_2	α
XY at 700°C & 250-400 MPa	1.09648E-13	2.218	6.45654E-15	4.637	3.5	0.2
Z at 700°C & 250-375 MPa	1.09648E-17	3.819	1.52757E-08	1.832	3	0.1

5. NUMERICAL MODELING AND FEM SIMULATION

5.1 Modeling Approach

Two validation tests have been simulated using the finite element method to demonstrate the viability of the creep damage model for additive manufactured nickel alloy 718 using the validated models. In these simulations, the creep life predictions are made by utilizing the usercreep based on CDM and the necking behavior during creep loading is simulated using the non-linear static analysis method. To incorporate material plasticity and damage, material non-linearity is assumed and modeled using bi-linear elasto-plastic stress-strain curves obtained from test data.

5.2 Finite element model setup

5.2.1 Geometry, mesh and boundary conditions

According to ASTM E139[2] standard test methods for conducting creep, a standard tensile creep specimen is modeled as shown in fig. an axisymmetric mesh with element type CAX4R for a cylindrical specimen is created to setup the creep test.

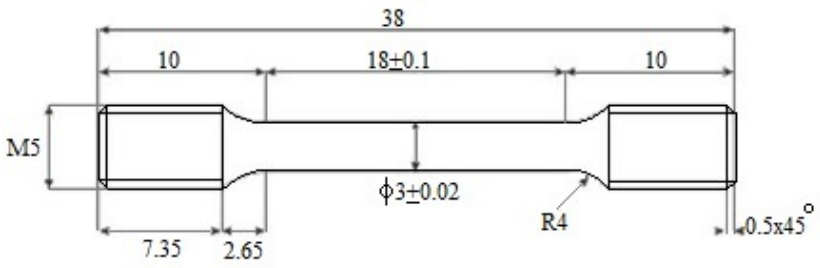

Figure 5.1. Creep test specimen.[20]

Testing standards suggest the use of cylindrical or square section specimens. A sub-size specimen ($3 < d_0 < 5mm$) is used to simulate the creep test in this report with a gauge length of 18 mm. A linear hex mesh is created to reduce computation time and decrease the node count.

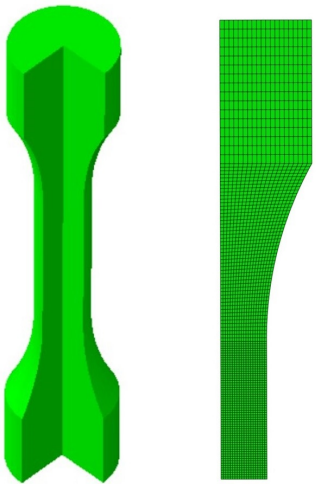

Figure 5.2. CAD used for the FEM simulation Cylindrical specimen geometry and Axisymmetric mesh.

For implementing the creep damage model in a FE simulation, determining a small enough mesh size requires a mesh convergence study to obtain the desired accuracy. For the FE simulation, a linear type of mesh elements is used which has four integration points where stress values are computed.

Figure 5.3. Boundary conditions.

The average stress values are computed to get a single value associated with the center node. For different mesh sizes, un-averaged von-mises stress plots are studied at element boundaries to evaluate convergence. A discontinuous contour along the element edges signify that the mesh is coarse.

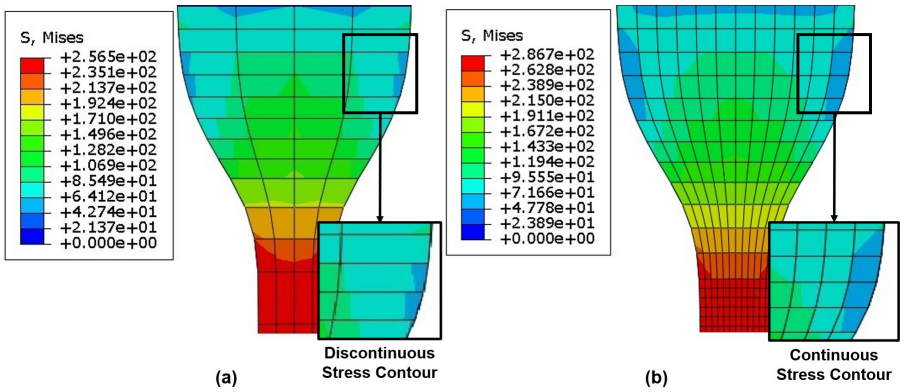

Figure 5.4. Contour plot of von Mises stress for (a) coarse and (b) fine mesh, without averaging at nodes.

It can be seen from the non-averaged mises stress contours above that for a coarser mesh, the contour lines are discontinuous along the specified element edges. Although when adopting a finer mesh, the discontinuities are no longer observed.

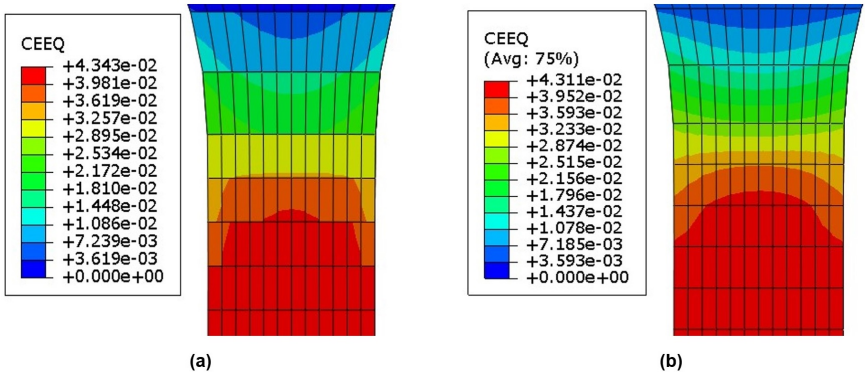

Figure 5.5. Contour plot of von Mises stress with and without averaging for a 3D mesh.

A plot of averaged vs non-averaged equivalent creep for a converged mesh is shown below. Contour discontinuities are not seen here which signifies the mesh size is optimum for convergence and a better solution accuracy.

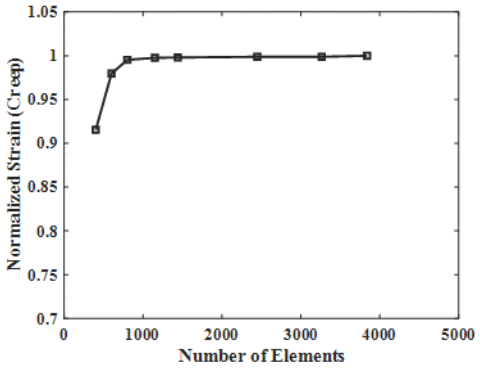

Figure 5.6. Mesh convergence plot.

To support the convergence study, normalized maximum mises stress is plotted against the number of elements. The mesh convergence plot ensures the solution accuracy by giving us the element size range for which the solution is not affected. In this case, for a mesh size with smallest element size around 0.5mm for solid brick elements, we see minimum change in the maximum mises stress values. Similarly. The smallest element size for axisymmetric element used in this report is 0.15 mm.

5.3 Additive manufactured nickel alloy 718 creep test Results

5.3.1 Single element test results

A damage evolution comparison is performed for the additive manufactured 718 alloys using the single element test to compare the damage prediction of both models. For applied stress of 515 MPa, constants for the Z orientation were used to calculate the damage and rupture time.

A similar behavior is observed for the CDM model comparison which was observed for traditionally manufactured nickel alloy 718 and stainless steel 316, for damage evolution. The rupture time predicted by the K-R model for the applied stress is 262.05 hours and the rupture time predicted by the L-M model is 214.12 hours.

To compare the difference in creep strain calculations for a 4 node and an 8 node element, the same single element test is performed for both element types using the L-M model CDM.

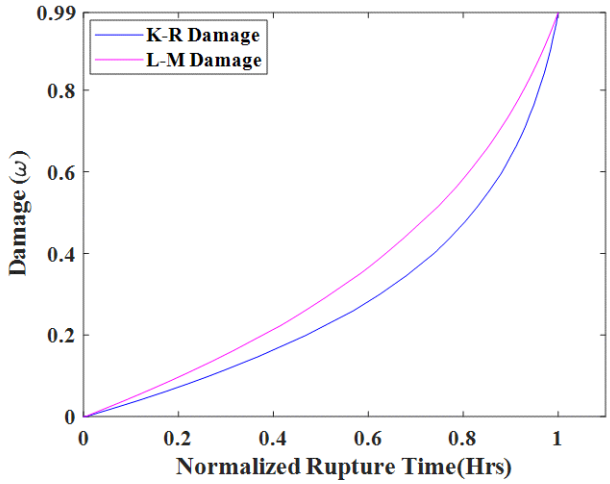

Figure 5.7. Damage evolution: K-R vs L-M for Z orientation AM 718.

It was observed that the 4 node element type gives a more accurate rupture time as compared to the 8 node element type.

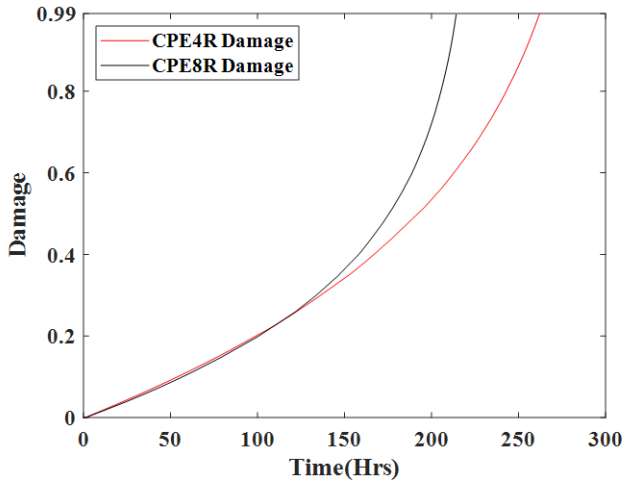

Figure 5.8. Dependence of node count on damage and rupture calculations for AM 718 using L-M model.

This test was performed for the Z orientation specimen 3. Both the models are under-predicting the rupture time as the results are calculated for a single element and plastic deformation is not incorporated.

5.3.2 Creep test results: K-R model

The K-R model was used to simulate the creep test. The focus was to achieve test accurate results and good creep strain and damage predictions.

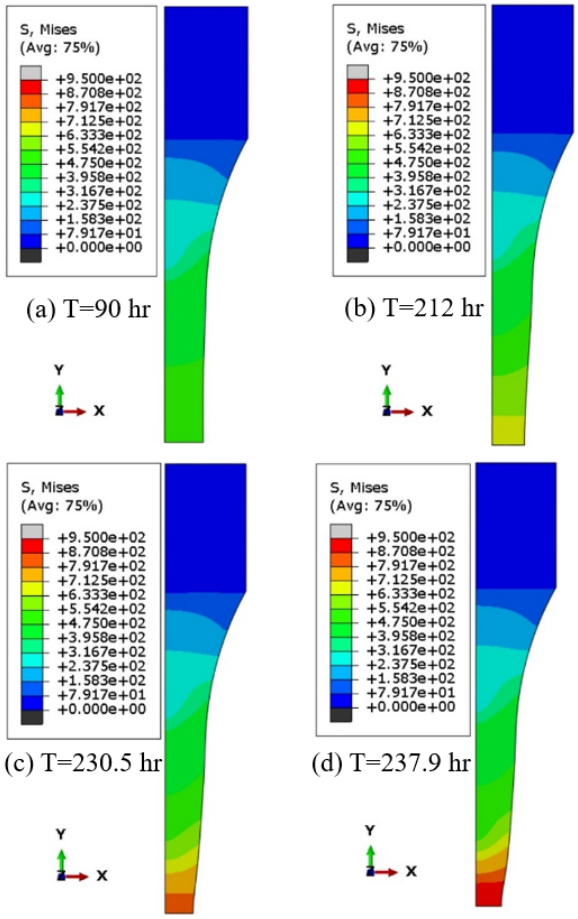

Figure 5.9. Von mises stress contour for AM 718.

The creep strain calculated was plotted against the available test data for L-PBF manufactured specimen.

Stress sensitivity can be observed for the K-R model. An exponential increase in creep strain is seen as the necking occurs. The damage plots show that the K-R model predicted rupture sooner than it occurred when compared to the experimental data.

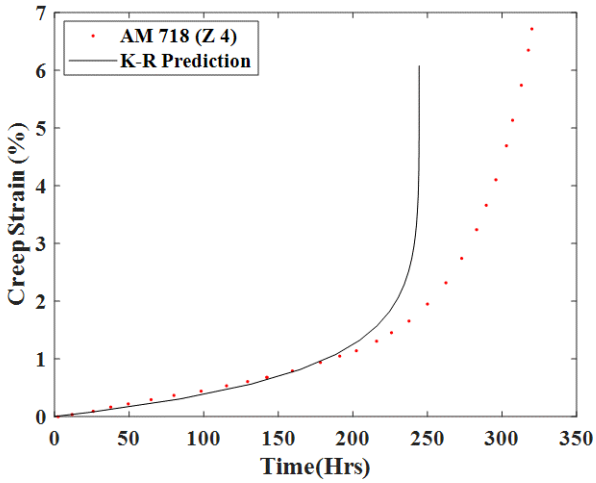

Figure 5.10. Creep strain validation curve for K-R model compared to the experimental AM 718 Z orientation specimen 4 creep data.

5.3.3 Creep test results: L-M model

For the L-M model, similar test setup was used to simulate the creep test. It is observed that necking is more prominent when using the L-M model.

L-M model is observed to overcome the stress sensitivity issue with the K-R model. The solution dependent variable (SDV)s represents the equivalent strain and damage contour for the test specimen.

Creep strain prediction for the additive manufactured nickel alloy 718 is accurate for the L-M model than the K-R model. It is observed that the K-R model rupture time predictions are less than the actual rupture time and on the other hand for the L-M model the rupture times predicted for Z orientation are very high but for XY orientation it is very accurate.

The creep strain is calculated by subtracting the elastic and plastic strain from total strain for the gauge length. Similar to strain gauge calculations, the change in length is calculated and thus calculating the total strain. Using the material parameters estimated by the regression curve fitting, the present model can be utilized to simulate secondary and tertiary creep behavior for additive manufactured metals.

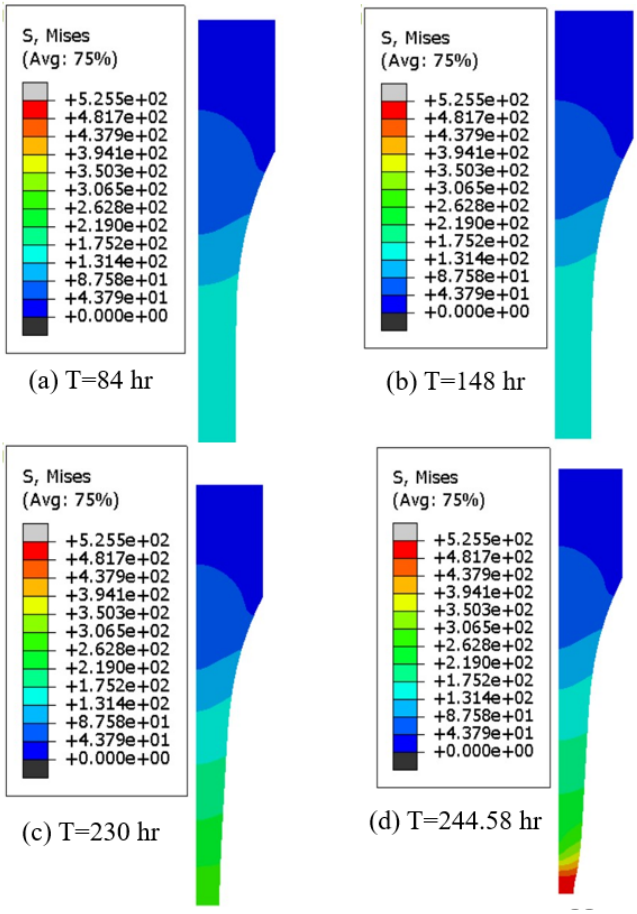

Figure 5.11. Von mises stress contour for AM 718.

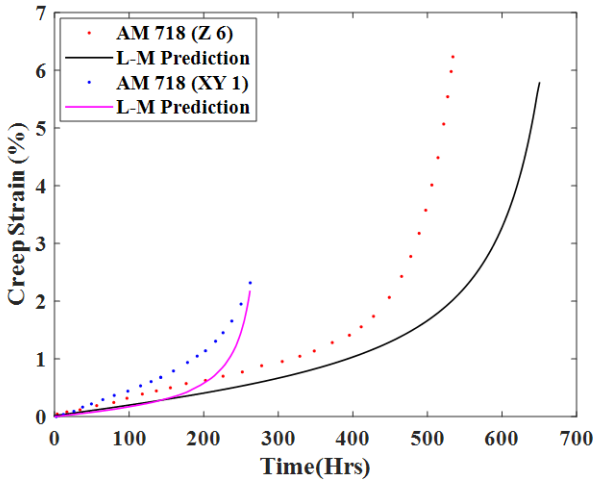

Figure 5.12. Creep strain validation curve for L-M model compared to experimental AM718 creep data.

6. CONCLUSIONS

The major conclusions are summarized as follows.

- A continuum damage mechanics (CDM) approach is employed by implementing a user-defined subroutine formulated to accurately capture the creep mechanisms. Using a calibration code, the material constants are determined.

- Using the multi-regime Liu-Murakami (L-M) and Kachanov-Rabotnov (K-R) isotropic creep damage formulation, creep deformation and rupture tests of both the secondary and tertiary creep behaviors are modeled.

- A single element FE model is used to validate the model constants. Creep strain prediction and damage evolution are calculated for 316 stainless steel at 240-300 MPa at 600°C, and nickel alloy 718 at 700-900MPa at 620°C. Temperature and stress dependence is captured by calculating constants at different temperatures, using the experimental creep test data. The user subroutine shows good accuracy at predicting creep strain at high stress and temperature. Damage variables (ω) and (q_2) are calculated for the best fit with overall creep curves. Multiaxiality constant α varies between 0.1 to 0.5 which gives consistent failure lives with the experimental results.

- A full-scale axisymmetric FE model is used to simulate the creep test and the capacity of the model to predict necking, creep damage, and creep-rupture life. The predicted creep curves are in good agreement with experimental data for L-PBF manufactured nickel alloy 718.

- The validated K-R and L-M models are implemented in the FE user subroutine to predict the creep behavior of additive manufactured nickel alloy 718 creep test specimen. Based on the material calibration method and the CDM model presented in this work, reliable creep predictions can be made for 3D printed alloys.

7. RECOMMENDATIONS

Creep model limitations: Although the current model is capable of predicting creep life, there are a few limitations of the work.

- The material constants estimated using regression curve fitting can be improved with the inclusion of more creep data points to avoid over prediction. Current model uses less data points to calculate the creep constants for 3D printed material.
- The work represents a phenomenological constitutive model which does not incorporate the micro/nanoscale creep occurring at the grain structure level.
- Current work considered a single damage constitutive model to estimate the creep deformation. The damage evolution solely depends on a single damage rate equation thus leading to stress sensitivity and over predictions.
- Material constant calibration process to estimate tertiary creep constants is performed using FE modeling. The damage evolution is thus restricted to the FE solver's capability to interpolate the results and FE model setup might be subjected to convergence issues.

The current model can be further implemented as follows,

- Conduct creep tests for the additive manufactured nickel alloy material at different stress and temperature levels. Gather strain rate and rupture datapoints for better curve fitting and material constant estimation for different stresses and temperatures.
- Additive manufactured materials differ in the grain structure formulation when compared to wrought material. A mechanistic constitutive model development approach can be implemented to incorporate the effect of creep damage at the microstructure level.
- Multiple damage parameter CDM models can be implemented for more accurate creep and damage predictions.

- Optimization techniques can be utilized to calibrate the tertiary creep model constants. Inclusion on numerical methods to predict the damage evolution can improve the creep prediction capability of the model.
- For specimen produced by different 3D printing process, relationship between the constitutive model parameters can be determined with extensive testing for creep.

REFERENCES

[1] *Data sheet: In718-0405 powder for additive manufacturing (pdf)*. Tech. rep. Part number: H-5800-1052, Accessed on 4/14/2021. Renishaw. URL: https://resources.renishaw.com/en/details/data-sheet-in718-0405-powder-for-additive-manufacturing--94192.

[2] ASTM E139-11(2018). "Standard Test Methods for Conducting Creep, Creep-Rupture, and Stress-Rupture Tests of Metallic Materials, ASTM International, West Conshohocken". In: (2018). URL: http://www.astm.org/cgi-bin/resolver.cgi?E139.

[3] R. Goodridge and S. Ziegelmeier. "7 - Powder bed fusion of polymers". In: *Laser Additive Manufacturing*. Ed. by Milan Brandt. Woodhead Publishing Series in Electronic and Optical Materials. Woodhead Publishing, 2017, pp. 181–204. ISBN: 978-0-08-100433-3. DOI: https://doi.org/10.1016/B978-0-08-100433-3.00007-5. URL: https://www.sciencedirect.com/science/article/pii/B9780081004333000075.

[4] Mohammad Shafinul Haque. "An Adaptive Creep Modeling Approach Using Metamodeling". PhD dissertation. University of Texas at El Paso, 2018.

[5] Mohammad Shafinul Haque. "An improved sin-hyperbolic constitutive model for creep deformation and damage". Masters thesis. University of Texas at El Paso, 2015.

[6] Mohammad Shafinul Haque and Calvin Maurice Stewart. "The disparate data problem: The calibration of creep laws across test type and stress, temperature, and time scales". In: *Theoretical and Applied Fracture Mechanics* 100 (2019), pp. 251–268. ISSN: 0167-8442. DOI: https://doi.org/10.1016/j.tafmec.2019.01.018. URL: https://www.sciencedirect.com/science/article/pii/S0167844218301800.

[7] C. Hautfenne, S. Nardone, and E. Bruycker. "Influence of heat treatments and build orientation on the creep strength of additive manufactured IN718". In: The European Creep Collaborative Committee. 4th International ECCC Conference, Sept. 2017.

[8] D R Hayhurst. "The use of continuum damage mechanics in creep analysis for design". In: *The Journal of Strain Analysis for Engineering Design* 29.3 (1994), pp. 233–241. DOI: 10.1243/03093247V293233.

[9] Karlsson Hibbitt and Sorensen. *ABAQUS: Theory Manual*. Accessed on 03/25/2020. DS. Providence, R.I., 1992.

[10] T.H. Hyde et al. "Failure estimation of TIG butt-welded Inco718 sheets at 620°C under creep and plasticity conditions". In: *Computational Materials Science* 35.1 (2006), pp. 35–41. ISSN: 0927-0256. DOI: https://doi.org/10.1016/j.commatsci.2005.02.013. URL: https://www.sciencedirect.com/science/article/pii/S0927025605000947.

[11] Instron. *Creep Test*. Accessed on 04/14/2021. URL: https://www.instron.us/en-us/our-company/library/glossary/c/creep-test.

[12] Alena Kreitcberg et al. "Temperature- and Time-Dependent Mechanical Behavior of Post-Treated IN625 Alloy Processed by Laser Powder Bed Fusion". In: *Journal of Manufacturing and Materials Processing* 3.3 (2019). ISSN: 2504-4494. DOI: 10.3390/jmmp3030075. URL: https://www.mdpi.com/2504-4494/3/3/75.

[13] Yen-Ling Kuo, Toshiki Nagahari, and Koji Kakehi. "The Effect of Post-Processes on the Microstructure and Creep Properties of Alloy718 Built Up by Selective Laser Melting". In: *Materials* 11.6 (2018). ISSN: 1996-1944. DOI: 10.3390/ma11060996. URL: https://www.mdpi.com/1996-1944/11/6/996.

[14] TWI Ltd. *Creep and Creep Testing*. Accessed on 04/14/2021. URL: https://www.twi-global.com/technical-knowledge/job-knowledge/creep-and-creep-testing-081.

[15] Yanjin Lu et al. "Study on the microstructure, mechanical property and residual stress of SLM Inconel-718 alloy manufactured by differing island scanning strategy". In: *Optics Laser Technology* 75 (2015), pp. 197–206. ISSN: 0030-3992. DOI: https://doi.org/10.1016/j.optlastec.2015.07.009. URL: https://www.sciencedirect.com/science/article/pii/S0030399215002108.

[16] M. McGaw. "Cumulative Damage Concepts in Thermomechanical Fatigue". In: *Thermomechanical Fatigue Behavior of Materials , ed. H. Sehitoglu (West Conshohocken, PA: ASTM International, 1993)* (1993), pp. 144–156. DOI: https://doi.org/10.1520/STP24254S.

[17] Qinghua Meng and Zhenqing Wang. "Creep damage models and their applications for crack growth analysis in pipes: A review". In: *Engineering Fracture Mechanics* 205 (2019), pp. 547–576. ISSN: 0013-7944. DOI: https://doi.org/10.1016/j.engfracmech.2015.09.055. URL: https://www.sciencedirect.com/science/article/pii/S0013794416303137.

[18] Dr. Sushila Rani. "Common Failures in Gas Turbine Blade: A Critical Review". In: *International Journal of Engineering Sciences & Research Technology* 7.3 (Mar. 2018), pp. 799–803. DOI: 10.5281/zenodo.1207072. URL: https://doi.org/10.5281/zenodo.1207072.

[19] Ehsan Saberi et al. "Predicting stress and creep life in Inconel 718 blade-disk attachments". In: *Engineering Failure Analysis* 108 (2020), p. 104226. ISSN: 1350-6307. DOI: https://doi.org/10.1016/j.engfailanal.2019.104226. URL: https://www.sciencedirect.com/science/article/pii/S1350630719300299.

[20] S. Sanchez et al. "The creep behaviour of nickel alloy 718 manufactured by laser powder bed fusion". In: *Materials Design* 204 (2021), p. 109647. ISSN: 0264-1275. DOI: https://doi.org/10.1016/j.matdes.2021.109647. URL: https://www.sciencedirect.com/science/article/pii/S0264127521002008.

[21] V.N. Shlyannikov. "Critical distance for creep crack growth problems". In: *Engineering Fracture Mechanics* 176 (2017), pp. 126–143. ISSN: 0013-7944. DOI: https://doi.org/10.1016/j.engfracmech.2017.03.001. URL: https://www.sciencedirect.com/science/article/pii/S0013794417302436.

[22] C. M. Stewart and A. P. Gordon. "Modeling the Temperature Dependence of Tertiary Creep Damage of a Ni-Based Alloy". In: *ASME. J. Pressure Vessel Technology* 131(5) (2009). ISSN: 051406. DOI: https://doi.org/10.1115/1.3148086.

[23] C. Stewart et al. "Characterization of the Creep Deformation and Rupture Behavior of DS GTD-111 Using the Kachanov–Rabotnov Constitutive Model". In: *Journal of Engineering Materials and Technology-transactions of The Asme* 133 (2011), p. 021013.

[24] Calvin M Stewart. "A Hybrid Constitutive Model for Creep, Fatigue, And Creep-Fatigue Damage". PhD dissertation. University of Central Florida, 2013.

[25] Calvin M Stewart. "Tertiary Creep Damage Modeling Of A Transversely Isotropic Ni-based Superalloy". Masters thesis. University of Central Florida, 2009.

[26] Tarcila Sugahara et al. "Creep Behavior of the Inconel 718 Superalloy". In: *Diffusion in Solids and Liquids VII*. Vol. 326. Defect and Diffusion Forum. Trans Tech Publications Ltd, May 2012, pp. 509–514. DOI: 10.4028/www.scientific.net/DDF.326-328.509.

[27] David W. J. Tanner. "Life assessment of welded INCONEL 718 at high temperature." PhD dissertation. University of Nottingham, 2009.

[28] Christopher J. Hyde Thomas H. Hyde Wei Sun. *Applied Creep Mechanics*. McGraw Hill Professional, 2013. ISBN: 9780071828697.

[29] Z. Xu et al. "Effect of post processing on the creep performance of laser powder bed fused Inconel 718". In: *Additive Manufacturing* 24 (2018), pp. 486–497. ISSN: 2214-8604. DOI: https://doi.org/10.1016/j.addma.2018.10.027. URL: https://www.sciencedirect.com/science/article/pii/S2214860418305578.

[30] Zhengkai Xu et al. "Creep behaviour of inconel 718 processed by laser powder bed fusion". In: *Journal of Materials Processing Technology* 256 (2018), pp. 13–24. ISSN: 0924-0136. DOI: https://doi.org/10.1016/j.jmatprotec.2018.01.040. URL: https://www.sciencedirect.com/science/article/pii/S0924013618300414.

[31] Yi Zhang. "Multi-Scale Multi-Physics Modeling of Laser Powder Bed Fusion Process of Metallic Materials With Experiment Validation". PhD dissertation. Purdue University, 2018.

[32] Yi Zhang, Yeon-Gil Jung, and Jing Zhang. "Chapter Ten - Finite element modeling of fatigue properties". In: *Multiscale Modeling of Additively Manufactured Metals*. Ed. by Yi Zhang, Yeon-Gil Jung, and Jing Zhang. Additive Manufacturing Materials and Technologies. Elsevier, 2020, pp. 191–231. ISBN: 978-0-12-819600-7. DOI: https://doi.org/10.1016/B978-0-12-819600-7.00010-1. URL: https://www.sciencedirect.com/science/article/pii/B9780128196007000101.

PUBLICATIONS

List of Publications

- Dhamade,H G., Gulhane, A., and Zhang,J. (2021). "Creep Modeling of Nickel Based Superalloys." PowderMet2021/AMPM2021/Tungsten2021. (Pending)
- Dhamade,H G., and Zhang,J. (2021). "Creep Modeling of Nickel Based Superalloys." Material Science technology(MST),2021 (Pending)
- Harshal G Dhamade, Abhilash Gulhane, Jian Zhang, Bong-Gu Kim, Yeon-Gil Jung, Jing Zhang. "Creep Modeling of 3D Printed 718 Nickel Alloys." Additive Mfg. Modeling and Simulation: AM Materials, Processes, and Mechanics, MST20
- Harshal G Dhamade, Anudeep Padmanabhan, Abhilash Gulhane, and Jing Zhang. "Creep Modeling of 3D Printed IN 718 Superalloys." Modeling of Metal AM Materials, Components Processes, PowderMet2019/AMPM2019.

List of Poster Presentations

- Harshal G Dhamade, Vighnesh U Shetty and Jing Zhang, Creep Modeling of 3D Printed IN 718 Superalloys, Poster session presented at POWDERMET19.
- Harshal G Dhamade and Jing Zhang, Creep simulation of 3D printed IN718, IUPUI Research day, Indianapolis, IN 2018 2019

List of Presentations

- Creep Modeling in AM Nickel Alloy, Harshal G Dhamade and Jing Zhang, ASM Indianapolis Chapter 2, Spring Conference, West Lafayette
- Creep Modeling of 3D Printed 15-5PH stainless steel, ASM Indianapolis Chapter Spring Conference, Columbus, IN; February 2019

Awards

- National science foundation(NSF) student grant for PowderMet2021/AMPM2021/Tungsten2021.
- National science foundation(NSF) travel grant for MST2018.